TOPICAL REVIEW — Iron-based high temperature superconductors

Spin fluctuations and unconventional superconducting pairing in iron-based superconductors*

Yu Shun-Li(于顺利) and Li Jian-Xin(李建新)†

National Laboratory of Solid State Microstructures and Department of Physics, Nanjing University, Nanjing 210093, *China*

(Received 16 June 2013; revised manuscript received 24 June 2013)

In this article, we review the recent theoretical works on the spin fluctuations and superconductivity in iron-based superconductors. Using the fluctuation exchange approximation and multi-orbital tight-binding models, we study the characteristics of the spin fluctuations and the symmetries of the superconducting gaps for different iron-based superconductors. We explore the systems with both electron-like and hole-like Fermi surfaces (FS) and the systems with only the electron-like FS. We argue that the spin-fluctuation theories are successful in explaining at least the essential part of the problems, indicating that the spin fluctuation is the common origin of superconductivity in iron-based superconductors.

Keywords: iron-base superconductors, spin fluctuations, pairing symmetry

PACS: 74.70.Xa, 74.20.–z, 74.20.Rp **DOI:** 10.1088/1674-1056/22/8/087411

1. Introduction

The discovery of iron-based superconductors (FeSCs) is the most significant breakthrough in the study of the unconventional superconductivity in recent years. Many efforts from both the experimental and theoretical communities have been devoted to understanding the normal state properties, the pairing mechanism, and the gap symmetry of these materials since 2008.

The first material of FeSCs to show superconductivity is LaOFeP reported in 2006, whose superconducting transition temperature T_c is 7 K,[1] but it did not attract widespread attentions at that time because of its low T_c. In February 2008, the discovery of 26-K superconductivity in fluorine-doped LaFeAsO[2] and consequently the findings of other FeSCs with an even higher T_c,[3–9] which suggest that the FeSCs are high-temperature superconducting materials, mark the beginning of worldwide efforts to investigate this new family of superconductors. So far, the FeSCs have been extended to include a large variety of materials, and the family still keeps growing. According to their formulas, they are often classified as "1111", "122", "111", "11", "32522", and "42622" materials, and a new family $A_xFe_{2-y}Se_2$ (A stands for alkali metals K, Rb, Cs, Tl) is often called as "245" because of its parent compound $A_{0.8}Fe_{1.6}Se_2 \equiv A_2Fe_4Se_5$. To date, all but the 32522 family exhibit a clear evidence of superconductivity, with the highest transition temperatures up to 55 K–56 K in the 1111 family,[6,10,11] therefore it is the second family of high-T_c superconductors.

The FeSCs share many common properties with high-T_c cuprates. (i) They all have a layered crystal structure. In FeSCs, it is based on a planar layer of iron atoms joined by tetrahedrally coordinated pnictogen (P, As) or chalcogen (S, Se, Te) anions arranged in a stacked sequence separated by alkali, alkaline-earth or rare-earth, and oxygen/fluorine blocking layers. The superconductivity comes from these common iron layers, which are similar to the common copper–oxygen layers in high-T_c cuprates. (ii) In high-T_c cuprates and most of FeSCs, the parent compound of the material has a magnetic ground state, and the superconductivity evolves from the parent compound by doping electrons or holes into it. (iii) Many experimental and theoretical results suggest that both cuprates and FeSCs are unconventional superconductors with a spin singlet pairing (non-phononic pairing mechanism). (iv) Mainly due to the proximity of the superconducting state to the magnetic state of the parent compound, it is suggested that the Coulomb interaction between electrons is an important ingredient to understand the superconductivity and the related properties.

However, there are also some differences between cuprates and FeSCs. i) Most of the parent compounds of FeSCs are metals, while those of cuprates are Mott insulators. So the electron correlations in FeScs are weaker than those in cuprates. Usually, it is suggested that FeSCs are in the intermediate correlation regime. The magnetic order in FeSCs is a spin-density wave (SDW), which is different from the Heisenberg antiferromagnetism with a localized magnetism. ii) In cuprates, the spins of the Cu atoms are ordered antiferromagnetically, however the arrangements of the spins of the Fe atoms in FeSCs are much more complicated. The 1111, 122, and 111 parent compounds have a common collinear in-

*Project supported by the National Natural Science Foundation of China (Grant Nos. 91021001, 11190023, and 11204125) and the National Basic Research Program of China (Grants Nos. 2011CB922101 and 2011CB605902).

†Corresponding author. E-mail: jxli@nju.edu.cn

© 2013 Chinese Physical Society and IOP Publishing Ltd

plane magnetic structure in which the spins are ordered antiferromagnetically in one Fe–Fe direction but ferromagnetically in the other direction.[12–15] $Fe_{1+y}Te$ in the 11 family shows the so called bicollinear spin order in which the spins are ordered ferromagnetically along a diagonal direction and antiferromagnetically along the other diagonal direction on the Fe square lattice.[16,17] The 245 family shows a $\sqrt{5}\times\sqrt{5}$ block-type antiferromagnetic structure due to the vacancies of the Fe atoms.[18,19] iii) The cuprates are single orbital systems, however the FeSCs are multi-orbital systems in which all the 3d orbitals (at least the t_{2g} orbitals) are important in the determination of the low-energy electron structures (see Fig. 1). iv) Due to the multi-band structure, the Fermi surface (FS) in FeSCs is much more complex than that in cuprates which have only a single FS. Except for some special materials, the FeSCs have five FS's (three hole-like ones and two electron-like ones).

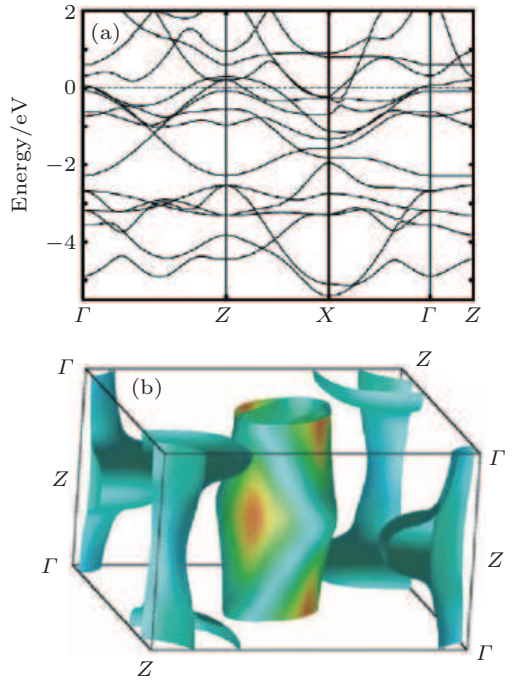


Fig. 1. (a) Calculated LDA band structure and (b) Fermi surface of $BaFe_2As_2$.[23]

The typical phase diagrams of FeSCs ($BaFe_{2-x}Ni_xAs_2$, electron doping;[20] $Ba_{1-x}K_xFe_2As_2$, hole doping[21]) are shown in Fig. 2. Below the Neel temperature, the long-range antiferromagnetic (AF) order starts to develop with a small moment per atom. With the electron or hole doping, the antiferromagnetic order in the parent compound is suppressed and superconductivity emerges. But in the underdoped regime, the SDW and superconductivity are suggested to coexist in an extended range of compositions. On the other hand, in a range of small dopings, $BaFe_{2-x}Ni_xAs_2$ shows a slightly difference between the structural and the magnetic phase transition temperatures. One can find that the phase diagram of iron-based superconductors is very similar to that of cuprates shown in Fig. 3, except that the undoped parent compound of cuprates is an antiferromagnetic Mott insulator while the iron-based material is a semimetal with a spin density wave. A major feature of these phase diagrams is that the superconducting phase is proximity to (or even coexists with) the magnetic order phase, suggesting that the spin fluctuations may be related to the superconductivity in FeSCs.

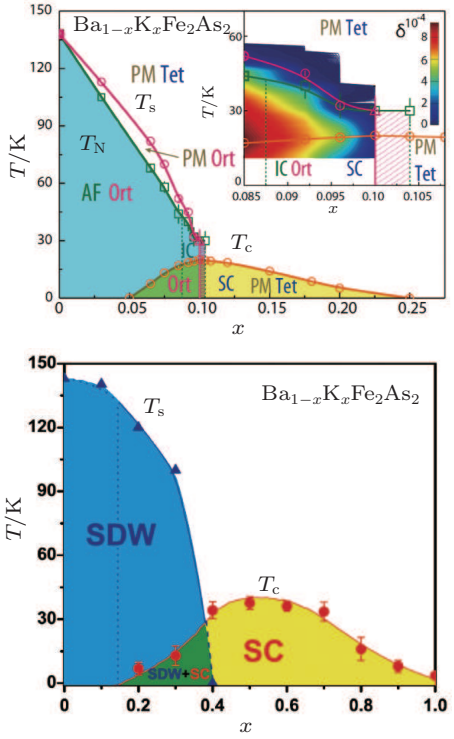


Fig. 2. The typical phase diagrams for 122 families. (a) Phase diagram of $BaFe_{2-x}Ni_xAs_2$. The PM Tet, PM Ort, AF Ort, and IC Ort are paramagnetic tetragonal, paramagnetic orthorhombic, AF orthorhombic, and incommensurate AF orthorhombic phases, respectively.[20] (b) Phase diagram of $Ba_{1-x}K_xFe_2As_2$, where T_s denotes the temperature of the simultaneous structural and magnetic transition.[21]

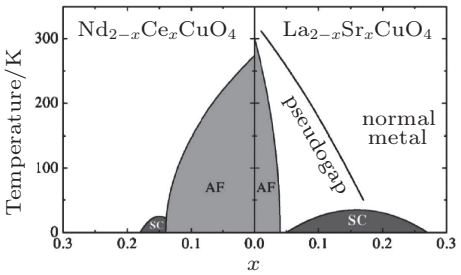


Fig. 3. Schematic phase diagram of high-T_c cuprate superconductors showing electron doping (left side) and hole doping (right side).[22]

2. Multi-orbital models

The first-principle calculations have shown that the energy bands near the Fermi surface are mainly contributed by the Fe 3d orbitals, together with some contribution from As p orbitals, within several eV of the Fermi level. In the FeAs layer, the Fe atoms form a square lattice and an Fe atom is coordinated by four As atoms in a tetrahedron. In fact, there are

two Fe atoms in each unit cell due to the staggered arrangement of the As ions above and below the square plaquette of Fe. Due to the direct Fe–Fe bonds and the hybridization with the As 4p orbitals, the Fe 3d orbitals form a complex band structure. But, as pointed out by Mazin,[24] it is in fact relatively simple to unfold the band structure to the extended Brillouin zone (BZ) corresponding to the one Fe unit cell. Thus, several simplified tight-binding models have been proposed, ranging from the simplest two-orbital models including only the d_{xz} and d_{yz} orbitals of the Fe atom, the three-orbital models by including the d_{xy} orbital into the two-orbital models, to the more sophisticated five-orbital model including all the five 3d orbitals of the Fe atom. The five-orbital model can be directly derived from the LDA results by using the maximally-localized Wannier function representation.

2.1. Two-orbital model

The band structure calculations have shown that the contribution to the energy bands near the Fermi level in fact comes mainly from the d_{xz}, d_{yz}, and d_{xy} orbitals (the direct Fe–Fe bonds along the x and y axes) of the Fe atoms. Based upon this result and by making a further approximation that the role of the d_{xy} orbital can be replaced by a next-near-neighbor hybridization between the d_{xz} and d_{yz} orbitals, Raghu *et al.* proposed a two-orbital model by including the two degenerate d_{xz} and d_{yz} orbitals.[25]

The tight-binding parameters of this two-orbital model are illustrated in Fig. 4. If we introduce a two-component field operator $\psi^{\dagger}_{\sigma}(\boldsymbol{k}) = [c^{\dagger}_{xz\sigma}(\boldsymbol{k}), c^{\dagger}_{yz\sigma}(\boldsymbol{k})]$, where $c^{\dagger}_{xz\sigma}(\boldsymbol{k})$ ($c^{\dagger}_{yz\sigma}(\boldsymbol{k})$) creates a d_{xz} (d_{yz}) electron with spin σ and wave vector $\boldsymbol{k}$, then the tight-binding Hamiltonian can be written as

$$H_0 = \sum_{\boldsymbol{k},\sigma} \psi^{\dagger}_{\sigma}(\boldsymbol{k}) \boldsymbol{M}(\boldsymbol{k}) \psi_{\sigma}(\boldsymbol{k}), \tag{1}$$

where $\boldsymbol{M}(\boldsymbol{k})$ is a 2×2 matrix. The elements of $\boldsymbol{M}(\boldsymbol{k})$ are given by

$$\begin{aligned} M_{11}(\boldsymbol{k}) &= -2t_1\cos(k_x) - 2t_2\cos(k_y) \\ &\quad -4t_3\cos(k_x)\cos(k_y), \end{aligned} \tag{2}$$

$$\begin{aligned} M_{22}(\boldsymbol{k}) &= -2t_2\cos(k_x) - 2t_1\cos(k_y) \\ &\quad -4t_3\cos(k_x)\cos(k_y), \end{aligned} \tag{3}$$

$$M_{12}(\boldsymbol{k}) = M_{21}(\boldsymbol{k}) = -2t_4\sin(k_x)\sin(k_y). \tag{4}$$

To reproduce the characters of the FS calculated by the LDA approximations, one can set $t_1 = -1, t_2 = 1.3, t_3 = t_4 = -0.85$, in units of $|t_1|$.[25] Figure 5 shows the band structure and the FS of the two-orbital model. In the two-Fe/cell BZ shown in Fig. 5(d), there are two hole Fermi pockets α_1 and α_2 and two electron Fermi pockets β_1 and β_2, which qualitatively agrees with the LDA results.

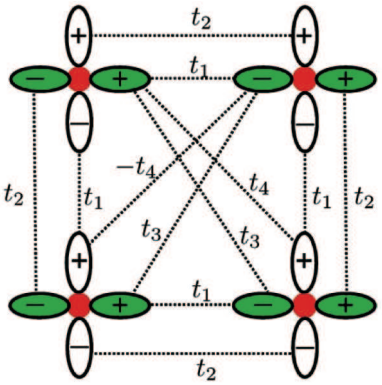


Fig. 4. Schematic figure showing the hopping parameters in the two-orbital model. The projections of the d_{xz} (d_{yz}) orbitals onto the xy plane are depicted in green (white). Here t_1 is the nearest-neighbor hopping between σ orbitals and t_2 is the nearest-neighbor hopping between π orbitals. The next-nearest-neighbor hopping t_4 between different orbitals and the next-nearest-neighbor hopping t_3 between the similar orbitals are also included.[25]

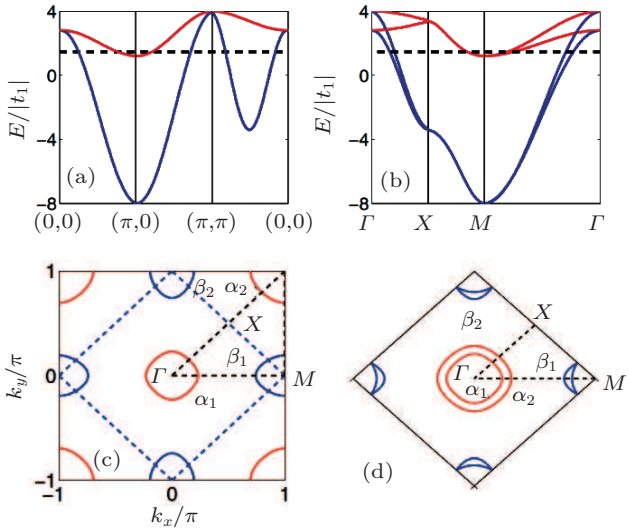


Fig. 5. (a) Band structure of the two-band model with $t_1 = -1, t_2 = 1.3$, $t_3 = t_4 = -0.85$, plotted along path $(0,0) \to (\pi,0) \to (\pi,\pi) \to (0,0)$ shown by the black dashed lines in panel (c). (b) Band structure folded to the original BZ, with the Γ, X, M defined in the original BZ as shown in panel (d). (c) Fermi surface of the two-orbital model in the one-Fe/cell BZ. (d) Fermi surface folded down into the two-Fe/cell BZ.[25]

2.2. Three-orbital model

The two-orbital model has some deficiencies. The first one is that one of the hole Fermi pockets is displaced from the $(0,0)$ point to the (π,π) point in the unfolded (one-Fe/cell) Brillouin zone in this model. The second one is that it misses the d_{xy} orbital character on the electron Fermi pockets. Thus, it has been argued that at least three orbitals are needed to describe the physical properties of the FeSCs.

The three-orbital model was first proposed by Lee and Wen[26] based on the symmetry properties of the Fe–As planes and the LDA results. Similar to the above discussion of the two-orbital model, one can define a three-component field operator $\psi^{\dagger}_{\sigma}(\boldsymbol{k}) = [c^{\dagger}_{xz\sigma}(\boldsymbol{k}), c^{\dagger}_{yz\sigma}(\boldsymbol{k}), c^{\dagger}_{xy\sigma}(\boldsymbol{k})]$. Then, the Hamiltonian has the same form as Eq. (1), but here $\boldsymbol{M}(\boldsymbol{k})$ is a 3×3 matrix. As pointed out in Ref. [26], the Fe–As (or Fe–Se)

plane is invariant under a translation along the x or y direction followed by a reflexion about the x–y plane. So, the momentum should be understood as a pseudocrystal momentum, i.e., $c_{xz}(\boldsymbol{k})$ and $c_{yz}(\boldsymbol{k})$ with conventional crystal momentum $\boldsymbol{k}+\boldsymbol{Q}$ and $c_{xy}(\boldsymbol{k})$ with crystal momentum $\boldsymbol{k}$, where $\boldsymbol{Q}=(\pi,\pi)$.

Considering the nearest-neighbor and the next-nearest-neighbor hoppings for all three orbitals, one will obtain the elements of $\boldsymbol{M}(\boldsymbol{k})$ as followings:[27]

$$\begin{aligned} M_{11}(\boldsymbol{k}) &= 2t_2\cos k_x + 2t_1\cos k_y \\ &\quad + 4t_3\cos k_x\cos k_y - \mu, \qquad (5)\\ M_{22}(\boldsymbol{k}) &= 2t_1\cos k_x + 2t_2\cos k_y \\ &\quad + 4t_3\cos k_x\cos k_y - \mu, \qquad (6)\\ M_{33}(\boldsymbol{k}) &= 2t_5(\cos k_x + \cos k_y) \\ &\quad + 4t_6\cos k_x\cos k_y + \Delta_{xy} - \mu, \qquad (7)\\ M_{12}(\boldsymbol{k}) &= M_{21}(\boldsymbol{k}) = 4t_4\sin k_x\sin k_y, \qquad (8)\\ M_{13}(\boldsymbol{k}) &= M_{31}^{*}(\boldsymbol{k}) = 2\mathrm{i}t_7\sin k_x + 4\mathrm{i}t_8\sin k_x\cos k_y, \qquad (9)\\ M_{23}(\boldsymbol{k}) &= M_{32}^{*}(\boldsymbol{k}) = 2\mathrm{i}t_7\sin k_y + 4\mathrm{i}t_8\sin k_y\cos k_x, \qquad (10) \end{aligned}$$

where μ is the chemical potential, and Δ_{xy} is the energy difference between the d_{xy} and the degenerate d_{xz}/d_{yz} orbitals.

The three-orbital model was used to calculate some physical properties of the FeSCs[28,29] soon after it was proposed. But, at that time, it contained a spurious hole-pocket FS around the M point in the one-Fe/cell BZ as the two-orbital model does. Later on, Daghofer *et al.* proposed a set of elegant parameters (see Table 1) to entirely remove this spurious FS.[27] The corresponding band structure and FS are shown in Fig. 6.

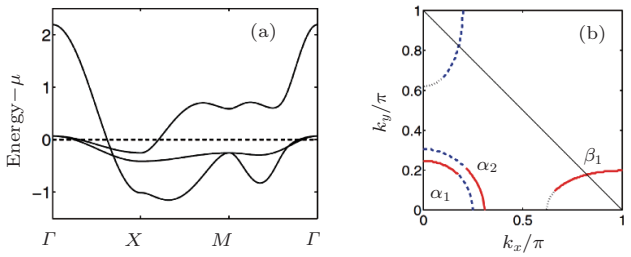


Fig. 6. (a) Band structure and (b) FS of the three-orbital model in the unfolded BZ, with parameters listed in Table 1.[27]

Table 1. Tight-binding parameters of the three-orbital model in units of eV.

t_1	t_2	t_3	t_4	t_5	t_6	t_7	t_8	Δ_{xy}
0.02	0.06	0.03	−0.01	0.2	0.3	−0.2	$-t_7/2$	0.4

2.3. Interactions between electrons

As discussed above, experiments suggest that the Coulomb interactions between electrons in FeSCs are in the intermediate-correlation regime. So, their physical properties should be understood by considering the electronic correlations. For a multi-orbital system, the Coulomb interaction is given by

$$\hat{V} = \frac{1}{2}\int \mathrm{d}\boldsymbol{x}\,\mathrm{d}\boldsymbol{y}\,v(\boldsymbol{x},\boldsymbol{y})\sum_{\sigma,\sigma'}\hat{\psi}_{\sigma}^{\dagger}(\boldsymbol{x})\hat{\psi}_{\sigma'}^{\dagger}(\boldsymbol{y})\hat{\psi}_{\sigma'}(\boldsymbol{y})\hat{\psi}_{\sigma}^{\dagger}(\boldsymbol{x}), \quad (11)$$

where the field operator $\hat{\psi}$ is defined as

$$\hat{\psi}_{\sigma}(\boldsymbol{x}) = \sum_{l=1}^{n}\phi_l(\boldsymbol{x})\hat{c}_{l\sigma}, \quad (12)$$

with l the orbital index. We can further express the Coulomb interaction as

$$\begin{aligned} \hat{V} &= \frac{1}{2}\sum_{i}\sum_{l_1l_2l_1'l_2'}\sum_{\sigma_1\sigma_2}\langle l_1\sigma_1, l_2\sigma_2|\hat{V}|l_2'\sigma_2, l_1'\sigma_1\rangle \\ &\quad \times \hat{c}_{il_1\sigma_1}^{\dagger}\hat{c}_{il_2\sigma_2}^{\dagger}\hat{c}_{il_2'\sigma_2}\hat{c}_{il_1'\sigma_1}, \qquad (13) \end{aligned}$$

where the element of the Coulombic interaction is

$$\begin{aligned} &\langle l_1\sigma_1, l_2\sigma_2|\hat{V}|l_2'\sigma_2, l_1'\sigma_1\rangle \\ &= \int \mathrm{d}\boldsymbol{x}\,\mathrm{d}\boldsymbol{y}\,v(\boldsymbol{x},\boldsymbol{y})\phi_{l_1\sigma_1}^{*}(\boldsymbol{x})\phi_{l_2\sigma_2}^{*}(\boldsymbol{y})\phi_{l_2'\sigma_2}(\boldsymbol{y})\phi_{l_1'\sigma_1}(\boldsymbol{x}). \qquad (14) \end{aligned}$$

Using the Kanamori parameters U, U', J, and J', which represent the intra-orbital Hubbard interaction, the inter-orbital Hubbard interaction, the Hund's rule coupling, and the pair-hopping integral,[30] we can write the Coulombic interaction as

$$\begin{aligned} H_{\mathrm{int}} &= \frac{1}{2}U\sum_{i,l,\sigma\neq\sigma'}c_{il\sigma}^{\dagger}c_{il\sigma'}^{\dagger}c_{il\sigma'}c_{il\sigma} \\ &\quad + \frac{1}{2}U'\sum_{i,l\neq l',\sigma,\sigma'}c_{il\sigma}^{\dagger}c_{il'\sigma'}^{\dagger}c_{il'\sigma'}c_{il\sigma} \\ &\quad + \frac{1}{2}J\sum_{i,l\neq l',\sigma,\sigma'}c_{il\sigma}^{\dagger}c_{il'\sigma'}^{\dagger}c_{il\sigma'}c_{il'\sigma} \\ &\quad + \frac{1}{2}J'\sum_{i,l\neq l',\sigma\neq\sigma'}c_{il\sigma}^{\dagger}c_{il\sigma'}^{\dagger}c_{il'\sigma'}c_{il'\sigma}, \qquad (15) \end{aligned}$$

where $U = \langle l\sigma, l\sigma'|\hat{V}|l\sigma', l\sigma\rangle$ for $\sigma\neq\sigma'$, $U' = \langle l\sigma, l'\sigma'|\hat{V}|l'\sigma', l\sigma\rangle$ for $l\neq l'$, $J = \langle l\sigma, l'\sigma'|\hat{V}|l\sigma', l'\sigma\rangle$ for $l\neq l'$, and $J' = \langle l\sigma, l\sigma'|\hat{V}|l'\sigma', l'\sigma\rangle$ for $l\neq l'$, $\sigma\neq\sigma'$. If the system has the rotational symmetry, U, U', J, and J' are not independent, they satisfy $J = J'$ and $U = U' + 2J$.[31,32]

3. Theory of the superconductivity mediated by spin fluctuations

Since the development of the BCS theory, it has been of interest to see whether the effective interaction responsible for the superconducting pairing could be mediated by excitations other than phonons. The effects of spin fluctuations on the superconductivity were first discussed by Berk and Schrieffer in 1966,[33] they found that the ferromagnetic spin fluctuation could induce a repulsive interaction and suppress the superconductivity effectively. On the other hand, the superfluidity of ^{3}He is an example that the pairing is due to the exchange of ferromagnetic spin fluctuations,

and consequently it results in a triplet p-wave pairing.[34,35] Since 1980s, superconductivity has been found in many systems with the parent compounds showing antiferromagnetism, such as heavy-fermion superconductors,[36,37] organic superconductors,[38,39] high-T_c cuprates,[40,41] and the latest iron-based superconductors.[42–44] This motivates researchers to develop the theory of superconductivity in which the Cooper pairing is mediated by antiferromagnetic spin fluctuations.

3.1. One-band Hubbard model and Cooper pairing mediated by spin fluctuations

The most classic model to describe the correlation between electrons is the Hubbard model, in which only the on-site Coulomb repulsion is included. The one-band Hubbard model contains only one orbital per site and is defined by

$$H = -t \sum_{\langle ij\rangle,\sigma} (c^{\dagger}_{i\sigma} c_{j\sigma} + \text{h.c.}) + U \sum_{i} n_{i\uparrow} n_{i\downarrow}, \tag{16}$$

where t is the nearest-neighbor hopping integral, and U is the on-site Coulomb interaction. Within the weak-coupling scheme, it is now well known that the Hubbard model on the square (cubic) lattice can give rise to the d-wave superconducting pairing. Then, the question arises, what causes the Cooper pairing in this repulsive Hubbard model? From the many-body theory, we know that the Cooper-pair instability arises in the particle–particle scattering channel with zero total momentum.[45] For the bare on-site Hubbard interaction, the electron–electron interaction is just the Hubbard interaction U, which is repulsive. After considering the exchanges of spin fluctuations, which are usually treated in the weak-coupling random-phase approximation (RPA) , as illustrated in Fig. 7(a) for the spin-singlet channel and Fig. 7(b) for the spin-triplet channel, one can obtain the effective electron–electron interaction potentials with zero frequency transfer

$$V_s(\boldsymbol{q}) = U + \frac{U^2\chi_0(\boldsymbol{q},0)}{1-U\chi_0(\boldsymbol{q},0)} + \frac{U^3\chi_0^2(\boldsymbol{q},0)}{1-U^2\chi_0^2(\boldsymbol{q},0)} \tag{17}$$

for the spin-singlet parings, and

$$V_t(\boldsymbol{q}) = -\frac{U^2\chi_0(\boldsymbol{q},0)}{1-U^2\chi_0^2(\boldsymbol{q},0)} \tag{18}$$

for the spin-triplet parings. Here, $\boldsymbol{q} = \boldsymbol{p} - \boldsymbol{p}'$ is the momentum transfer in the scattering of a pair of electrons from state $(\boldsymbol{p}, -\boldsymbol{p})$ to state $(\boldsymbol{p}', -\boldsymbol{p}')$, and $\chi_0(\boldsymbol{q}, \omega)$ is the wave-vector dependent susceptibility of the noninteracting electrons. For a square lattice, it has been shown that the spin-triplet pairing is not favored in the Hubbard model,[46] so we will just discuss the pairing in the spin-singlet channel in the followings. Now, one finds that the potential $V_s(\boldsymbol{q})$ gains a $\boldsymbol{q}$ dependence via the exchange of spin fluctuations. However, this effective particle–particle interaction is still positive, as shown in Fig. 8(a). Can such an interaction lead to the superconducting pairing? To answer this question, let us perform the Fourier transformation of $V_s(\boldsymbol{q})$ and study the distribution of the interaction potential in real space. The results are presented in Fig. 8(b). One can find that the interaction potential will oscillate between repulsion and attractive values depending on the relative distance of the two electrons. Therefore, if the two electrons can spatially arrange themselves to take advantage of the attractive regions of the interaction, then it is possible for them to pair. This Cooper pairing is mediated by spin fluctuations.

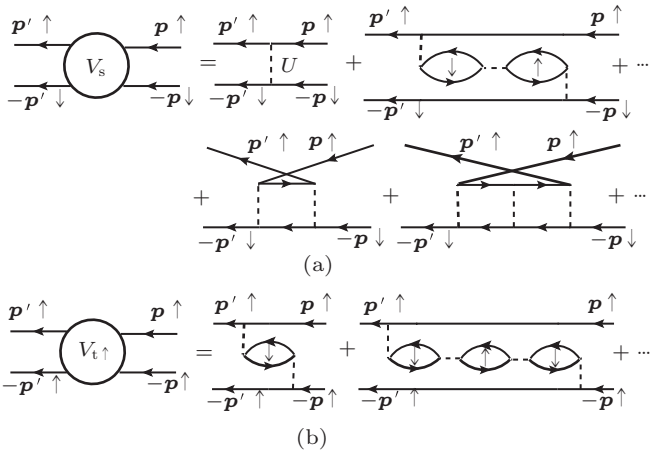


Fig. 7. Feynman diagrams illustrating the effective particle–particle interaction by exchanging the transverse and longitudinal spin fluctuations in (a) the spin-singlet channel and (b) the spin-triplet channel.

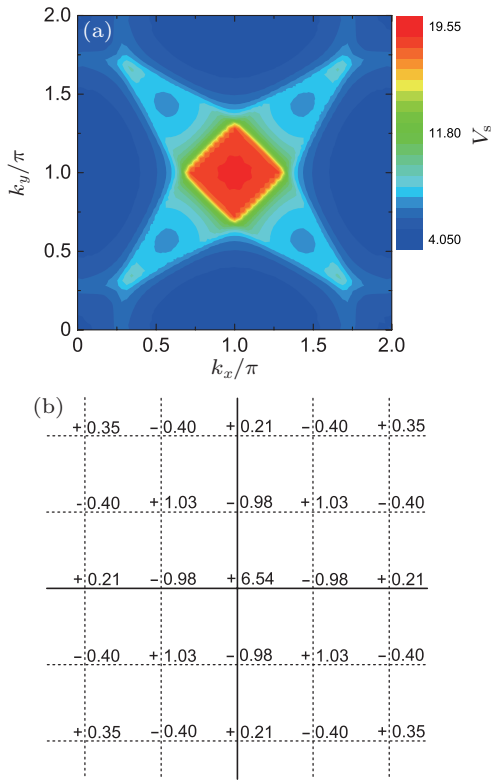


Fig. 8. (a) Effective electron–electron interaction potential $V_s(\boldsymbol{q})$ calculated from Eq. (17) with $t = 1$, the next-nearest-neighbor hopping $t' = -0.3$, $U = 2$, and 12% hole doping. (b) Fourier transformation of $V_s(\boldsymbol{q})$.

3.2. The d-wave superconductivity mediated by antiferromagnetic spin fluctuations

As discussed above, the exchange of the spin fluctuation with a wave vector $\boldsymbol{q}$ in the one-band Hubbard model may lead to the pairing of electrons. For a two-dimensional square lattice and with a finite hole doping, one can find that the spin fluctuation will peak at $\boldsymbol{q} = (\pi, \pi)$ (see also Fig. 8(a), in which the $\boldsymbol{q}$ structure of $V_{\rm s}$ is mainly determined by that of χ_0), which is right at the antiferromagnetic wavevector. Thus, it is the AFM spin fluctuation and is consistent with the experiments on high-$T_{\rm c}$ cuprates. Now, let us discuss what is the most favorable pairing symmetry mediated by AFM spin fluctuations.

To look for the most favorable pairing symmetry, one needs to solve the linear Eliashberg equation. In the case of a single band, it is given by

$$\Delta(\boldsymbol{k}) = -\frac{T}{N}\sum_{\boldsymbol{k}',n} V_{\rm s,t}(\boldsymbol{k}-\boldsymbol{k}')G(\boldsymbol{k}',-{\rm i}\omega_n) \times G(-\boldsymbol{k}',{\rm i}\omega_n)\Delta(\boldsymbol{k}'). \tag{19}$$

It describes the physical process in which a pair of electrons with momenta $\boldsymbol{k}$ and $-\boldsymbol{k}$ are scattered into the states of $\boldsymbol{k}'$ and $-\boldsymbol{k}'$ via the exchange of bosonic excitations. The effect of the exchange of bosonic excitations is represented by the effective interaction potential $V_{\rm s,t}(\boldsymbol{q})$ with $\boldsymbol{q} = \boldsymbol{k} - \boldsymbol{k}'$. In the weak-coupling regime, the Matsubara Green's function $\boldsymbol{G}(\boldsymbol{k}, {\rm i}\omega_n)$ can be approximated by the bare Green's function $G(\boldsymbol{k}, {\rm i}\omega_n) = [{\rm i}\omega_n - E(\boldsymbol{k})]^{-1}$ with $E(\boldsymbol{k}) = \sqrt{\varepsilon^2(\boldsymbol{k}) + \Delta^2(\boldsymbol{k})}$. After summing over the Matsubara frequency in Eq. (19), we get the usual BCS gap equation

$$\Delta(\boldsymbol{k}) = -\sum_{\boldsymbol{k}'} \frac{V(\boldsymbol{k}-\boldsymbol{k}')}{2E(\boldsymbol{k}')}\Delta(\boldsymbol{k}'). \tag{20}$$

In the case of the phonon-mediated pairing, the effective potential $V(\boldsymbol{q})$ is attractive (negative) and is approximately a constant V_0. Therefore, the s-wave pairing with a constant Δ_0 is obtained from Eq. (20). Now in the case of the spin-fluctuation-mediated pairing, $V(\boldsymbol{q})$ is repulsion (positive) and has a strong $\boldsymbol{q}$ dependence (Fig. 8(a)). If $V(\boldsymbol{q})$ has a strong peak at $\boldsymbol{q} = \boldsymbol{Q}$, then equation (20) can be approximated by $\Delta(\boldsymbol{k}) = -V(\boldsymbol{Q})\Delta(\boldsymbol{k}+\boldsymbol{Q})/2E(\boldsymbol{k}+\boldsymbol{Q})$. Consequently, the condition $\Delta(\boldsymbol{k}) = -\Delta(\boldsymbol{k}+\boldsymbol{Q})$ is required to get a solution for the gap equation, because $V(\boldsymbol{Q})$ is always positive for the repulsive interaction. If the electron pairings are mediated by AFM spin fluctuations, then $\boldsymbol{Q} = (\pi, \pi)$ and a $d_{x^2-y^2}$-wave pairing is favored in the two-dimensional square lattice, as shown in Fig. 9. This is applied to high-$T_{\rm c}$ cuprates in the framework that the superconducting pairing is mediated by AFM spin fluctuations.

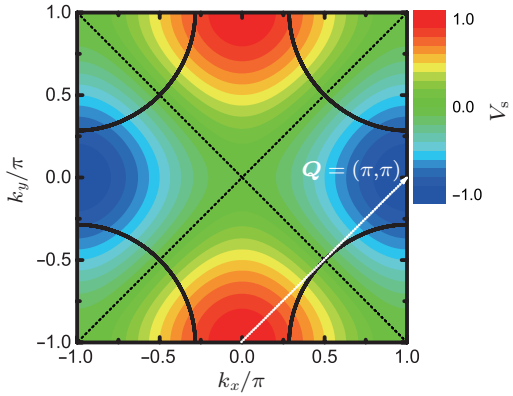


Fig. 9. The most favorable pairing function calculated using the result of $V_{\rm s}(\boldsymbol{q})$ shown in Fig. 8(a). It is of the $d_{x^2-y^2}$ symmetry. The dashed white line denotes the AFM wavevector $\boldsymbol{Q} = (\pi, \pi)$, the bold black line represents the Fermi surface, and the black dotted line gives the gap nodes. Note that the two gap functions connecting by $\boldsymbol{Q}$ have an opposite sign due to the repulsive interaction (see text).

3.3. Fluctuation exchange approximation

For a correlated electron system, it is more useful to go beyond the RPA approximation and consider the renormalization of the electron Green's function by the interactions self-consistently. One of the methods is the fluctuation exchange approximation (FLEX).[47,48] The FLEX approximation is formulated by using the conserving approximation scheme of Baym and Kadanoff.[49,50] The conserving approximations guarantee that the microscopic conservation laws for particle number, energy, and momentum are automatically fulfilled. The basic step in this approach is to derive the single-particle self-energy Σ by functional derivative of an approximate free-energy functional Φ with respect to the Green's function G, $\Sigma = \delta\Phi/\delta G$. The functional Φ in the FLEX approximation is shown in Fig. 10, which includes the contributions from the Hartree–Fock term, the longitudinal spin and charge fluctuations, the transverse spin fluctuations, and the particle–particle fluctuations. Note that the Fermion lines in Fig. 10 represent the renormalized Green's functions which will be determined self-consistently.

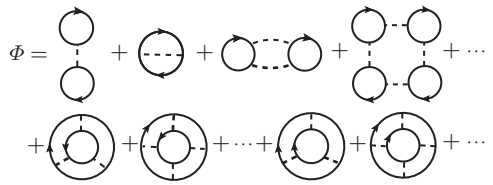


Fig. 10. Free energy functional for the FLEX approximation. The full lines represent the dressed Green's function, and the dashed lines represent the interaction.

For the two-dimensional Hubbard model, the self-energy in the FLEX approximation is given by

$$\Sigma(\boldsymbol{k}) = \frac{T}{N}\sum_{\boldsymbol{q}} V_{\rm eff}(\boldsymbol{k}-\boldsymbol{q})G(\boldsymbol{q}), \tag{21}$$

where the effective interaction reads

$$V_{\rm eff}(\boldsymbol{q}) = \frac{U^2\chi_0(\boldsymbol{q})}{1-U^2\chi_0^2(\boldsymbol{q})} + \frac{U^3\chi_0^2({\rm q})}{1-U\chi_0({\rm q})}. \tag{22}$$

Here we do not include the contributions from the particle–particle fluctuations which are not significant and usually ignored. The irreducible susceptibility is given by

$$\chi_0(q) = -\frac{T}{N}\sum_{k} G(k+q)G(k), \tag{23}$$

where T is the temperature, and $k \equiv (k, \mathrm{i}\omega_n)$ with $\omega_n = \pi T(2n+1)$. On the other hand, the renormalized Green's function G, the bare Green's function $G_0(k) = (\mathrm{i}\omega_n - \varepsilon_k)^{-1}$, and the self-energy Σ satisfy the Dyson equation

$$G^{-1}(k) = G_0^{-1}(k) - \Sigma(k). \tag{24}$$

Thus, equations (21)–(23) form a closed set of equations to be solved self-consistently.

We can generalize the FLEX approximation to the multi-orbital case.[51] Now, all the Green's functions and susceptibilities have an orbital dependence, and we can use a matrix representation. We consider an n-orbital system in which the interactions are described by Eq. (15). In this case, the Green's function $\hat{G}$ and the self-energy $\hat{\Sigma}$ can be expressed in an $n \times n$-matrix form, while the susceptibility $\hat{\chi}^0$ and the effective interaction $\hat{V}$ have an $n^2 \times n^2$-matrix form. Here, we use the alphabets with a hat to denote the matrices. Then, the Dyson equation is

$$\hat{G}(k)^{-1} = \hat{G}^0(k)^{-1} - \hat{\Sigma}(k), \tag{25}$$

where the self-energy is given by

$$\Sigma_{mn}(k) = \frac{T}{N}\sum_{q}\sum_{\mu\nu} V_{n\mu,m\nu}(q)G_{\mu\nu}(k-q), \tag{26}$$

and the bare Green's function reads

$$\hat{G}^0(k) = (\mathrm{i}\omega_n - \hat{M}_k + \mu)^{-1}. \tag{27}$$

The fluctuation exchange interaction is given by

$$\begin{aligned} V_{\mu m,n\nu}(q) = & \left\{ \frac{3}{2}U^{\mathrm{s}}[(1-\chi^0(q)U^{\mathrm{s}})^{-1} - 1]\chi^0(q)U^{\mathrm{s}} \right. \\ & + \frac{1}{2}U^{\mathrm{c}}[(1+\chi^0(q)U^{\mathrm{c}})^{-1} - 1]\chi^0(q)U^{\mathrm{c}} \\ & \left. + \frac{1}{2}(U^{\mathrm{s}}\chi^0(q)U^{\mathrm{s}} + U^{\mathrm{c}}\chi^0(q)U^{\mathrm{c}}) \right\}_{\mu m,n\nu}, \end{aligned} \tag{28}$$

where the irreducible susceptibility is given by

$$\chi^0_{\mu m,n\nu}(q) = -\frac{T}{N}\sum_{k} G_{n\mu}(k+q)G_{m\nu}(k). \tag{29}$$

The interaction matrices for the spin (charge) fluctuations, $\hat{U}^{\mathrm{s}}$ ($\hat{U}^{\mathrm{c}}$), are given as follows. For $i = j = k = l$, $U^{\mathrm{s}}_{ij,kl} = U$ ($U^{\mathrm{c}}_{ij,kl} = U$); for $i = j \neq k = l$, $U^{\mathrm{s}}_{ij,kl} = J$ ($U^{\mathrm{c}}_{ij,kl} = 2U' - J$); for $i = k$, $j = l$, and $i \neq j$, $U^{\mathrm{s}}_{ij,kl} = U'$ ($U^{\mathrm{c}}_{ij,kl} = -U' + 2J$); for $i = l$, $j = k$, and $i \neq j$, $U^{\mathrm{s}}_{ij,kl} = J$ ($U^{\mathrm{c}}_{ij,kl} = J$); for other cases, $U^{\mathrm{s}}_{ij,kl} = 0$ ($U^{\mathrm{c}}_{ij,kl} = 0$). Since the equations must be solved at fixed electronic density n, they are subject to the additional constraint

$$n(T) = \frac{T}{N}\sum_{k} \mathrm{e}^{\mathrm{i}\omega_n 0^+}\mathrm{Tr}\hat{G}(k, \mu(T)) = n, \tag{30}$$

where the chemical potential μ must be adjusted accordingly during the self-consistent calculation.

To study the superconducting pairing symmetry, we can solve the "Eliashberg" equation (the Eliashberg equation corresponds to the following equation with eigenvalue $\lambda = 1$) after obtaining the renormalized Green's function $\hat{G}$

$$\begin{aligned} \lambda\phi_{mn}(k) = & -\frac{T}{N}\sum_{q}\sum_{\alpha\beta}\sum_{\mu\nu} V^{\mathrm{s,t}}_{\alpha m,n\beta}(q)G_{\alpha\mu}(k-q) \\ & \times G_{\beta\nu}(q-k)\phi_{\mu\nu}(k-q), \end{aligned} \tag{31}$$

where the spin-singlet and spin-triplet pairing interactions $\hat{V}^{\mathrm{s}}$ and $\hat{V}^{\mathrm{t}}$ are given by

$$\begin{aligned} \hat{V}^{\mathrm{s}}(q) = & \frac{3}{2}\hat{U}^{\mathrm{s}}\hat{\chi}^{\mathrm{s}}(q)\hat{U}^{\mathrm{s}} - \frac{1}{2}\hat{U}^{\mathrm{c}}\hat{\chi}^{\mathrm{c}}(q)\hat{U}^{\mathrm{c}} \\ & + \frac{1}{2}(\hat{U}^{\mathrm{c}} + \hat{U}^{\mathrm{s}}), \end{aligned} \tag{32}$$

$$\begin{aligned} \hat{V}^{\mathrm{t}}(q) = & -\frac{1}{2}\hat{U}^{\mathrm{s}}\hat{\chi}^{\mathrm{s}}(q)\hat{U}^{\mathrm{s}} - \frac{1}{2}\hat{U}^{\mathrm{c}}\hat{\chi}^{\mathrm{c}}(q)\hat{U}^{\mathrm{c}} \\ & + \frac{1}{2}(\hat{U}^{\mathrm{c}} - \hat{U}^{\mathrm{s}}), \end{aligned} \tag{33}$$

with

$$\hat{\chi}^{\mathrm{s}}(q) = [\hat{I} - \hat{\chi}^0(q)\hat{U}^{\mathrm{s}}]^{-1}\hat{\chi}^0(q), \tag{34}$$

$$\hat{\chi}^{\mathrm{c}}(q) = [\hat{I} + \hat{\chi}^0(q)\hat{U}^{\mathrm{c}}]^{-1}\hat{\chi}^0(q). \tag{35}$$

The underlying physics contained in these equations has been discussed in Subsections 3.1 and 3.2. The most favorable superconducting pairing symmetry corresponds to the eigenvector $\phi_{mn}(k)$ with the largest eigenvalue λ.

4. Spin fluctuations and superconducting pairing in iron-based superconductors

At the early days of the discovery of iron-based superconductors, it has been shown by using the first-principle calculations that the electron–phonon coupling is not sufficient to explain the superconductivity in iron-based superconductors.[52] On the other hand, the experiments have shown that the superconducting state is proximity to the AFM spin-density-wave state, as discussed in Section 1. These suggest that the AFM spin fluctuations may play an important role in the superconductivity. In fact, Mazin *et al.* have argued that the AFM spin fluctuations in iron-based superconductors could lead to a superconducting state with a gap which has the opposite sign on the electron and hole pockets.[24] Here, we will only briefly review the spin-fluctuation mechanism of the superconducting pairing in iron-based superconductors.

4.1. Systems with both electron and hole pockets

4.1.1. FLEX calculations based on the two-orbital model

Let us start from the effective two-band model Hamiltonian described by Eq. (1). The interactions between electrons are described by Eq. (15).[53] Experimental data indicate that the undoped material of FeSCs behaves like a semimetal and exhibits itinerant antiferromagnetism. Thus, it is reasonable to consider the Coulomb interaction to be intermediate in this system. In this sense, the FLEX approach appears to be an adequate method. Here, the tight-binding parameters are $t_1 = -1.0$, $t_2 = 1.5$, $t_3 = -1.2$, and $t_4 = -0.95$ (in units of $|t_1|$). The corresponding energy band structure and FS with two chemical potentials $\mu = 0.74$ and 1.7 are shown in Fig. 11. Numerical calculations are carried out with a 32×32 k mesh in the one-Fe/cell BZ and 1024 Matsubara frequencies. The analytic continuation to the real frequency is carried out with the usual Padé approximant.[54]

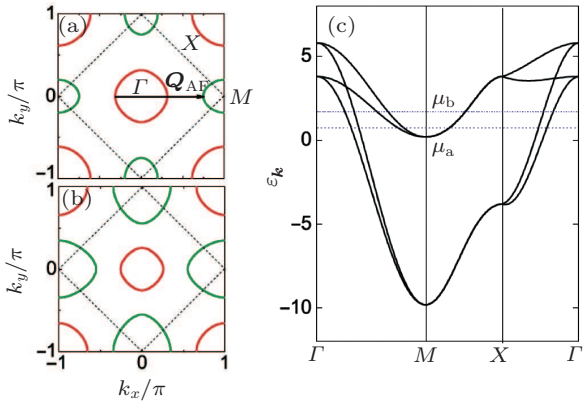


Fig. 11. Fermi surfaces of the two-band model in the extended (one-Fe/cell) BZ for (a) $\mu_a = 0.74$ and (b) $\mu_b = 1.7$. The thin dashed line denotes the folded BZ (two-Fe/cell) and the line with an arrow represents the nesting wave vector (see text). (c) The corresponding band structure (energy is in units of t_1) in the folded BZ.[53]

For $U > U'$, the spin fluctuations will dominate over the charge fluctuations, so we will only discuss the spin fluctuations in the following. In Fig. 12, the physical static spin susceptibility $\chi^s(\boldsymbol{q}, \omega = 0) = \sum_{\mu\nu} \chi^s_{\mu\nu,\mu\nu}(\boldsymbol{q}, \omega = 0)$ (for brevity, $\chi^s_{mn} = \chi^s_{mn,mn}$ is used hereafter) with a set of typical parameters $U = 5.5$, $U' = 4.0$, $J = J' = 1.0$, and $\mu = 0.74$ is presented. An obvious feature of χ^s is that it has dominant peaks around $(\pi, 0)$ and its symmetric points in the unfolded one-Fe/cell BZ. After checking the intra-band and the inter-band components χ^s_{22}, χ^s_{11}, and χ^s_{12} (not shown here), we find that this $(\pi, 0)$ spin fluctuation comes from the inter-band particle–hole excitations, which is essentially associated with the FS nesting between the hole and electron pockets, as indicated in Fig. 11(a).

The most favorable superconducting pairing symmetry at a fixed temperature is determined by solving the Eliashberg equation with the maximum eigenvalue. The calculated eigenvalues versus temperature for various possible pairing symmetries are plotted in Fig. 12(b). Firstly, one can see that the eigenvalue for the spin-triplet p-wave state is much smaller than that for the spin-singlet states. Therefore, we can safely rule out the possibility of the spin-triplet state in the present model. In the spin-singlet channel, the eigenvalue of the extended s-wave state is larger than that of the d-wave state, and they show a similar temperature dependence. In view of this tendency, although the maximum eigenvalue $\lambda = 1$ has not been reached yet, it is reasonable to consider the spin-singlet extended s-wave to be the most favorable state. The calculated k-space structures of the gap functions for both the electron and hole bands in the extended BZ are presented in Figs. 12(c) and 12(d), respectively. It has the same sign within each Fermi pocket, but the sign changes between the electron and hole pockets. This extended s-wave pairing has now been called as the $s_{\pm}$-wave pairing. It can be roughly fit by the gap function $\Delta(\boldsymbol{k}) \approx \cos k_x \cos k_y$.

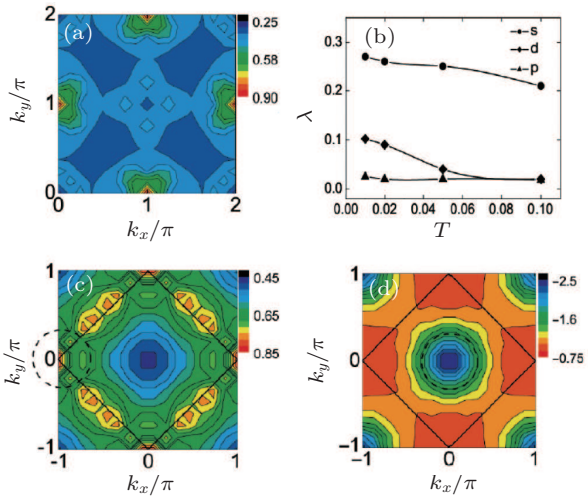


Fig. 12. (a) The $\boldsymbol{k}$ dependence of the static spin susceptibility (see text). (b) The temperature dependence of the eigenvalues for various pairing states. The $\boldsymbol{k}$ dependence of the gap functions corresponding to the largest eigenvalue for (c) the electron and (d) the hole Fermi pockets. The parameters are $U = 5.5$, $U' = 4.0$, $J = J' = 1.0$, and $\mu = 0.74$ at temperature $T = 0.01$.[53]

For another set of interaction parameters which has a large ratio of U/U', such as $U = 6.5$, $U' = 3.5$, $J = J' = 1.0$, and $\mu = 0.74$, we find that the physical spin susceptibility displays two sets of dominant peaks, with one still around $(\pi, 0)$ and the other around $(0.5\pi, 0.5\pi)$, as shown in Fig. 13(a). The new peak around $(0.5\pi, 0.5\pi)$ comes from the intra-band spin fluctuation which is enhanced largely by the intra-band Coulomb interaction U. In this case, the most favorable pairing symmetry is the d_{xy}-wave as shown in Fig. 13(b), and the corresponding gap functions in momentum space are displayed in Figs. 13(c) and 13(d). The U–U' phase diagram of the s-wave and d-wave pairing states is schematically shown

in Fig. 14. It shows clearly that the $s_{\pm}$-wave pairing is more favored with a relatively small ratio of U/U'.

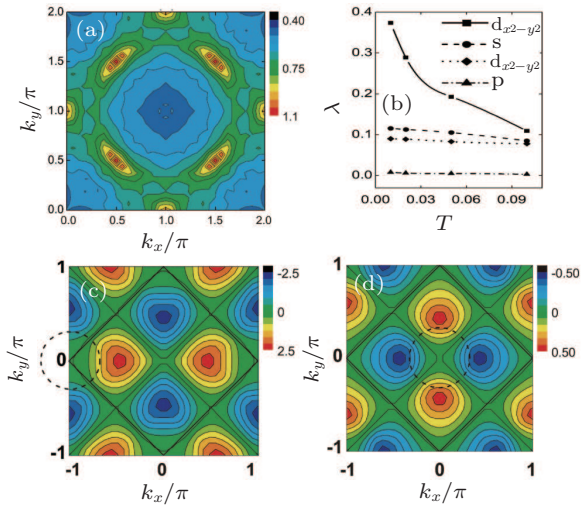


Fig. 13. (a) The $\boldsymbol{k}$ dependence of the static spin susceptibility for $U = 6.5$, $U' = 3.5$, $J = J' = 1$, and $\mu = 0.74$ at temperature $T = 0.01$. (b) The temperature dependence of the eigenvalues for various pairing states. The $\boldsymbol{k}$ dependence of the gap functions corresponding to the largest eigenvalue for (c) the electron and (d) the hole Fermi pockets.[53]

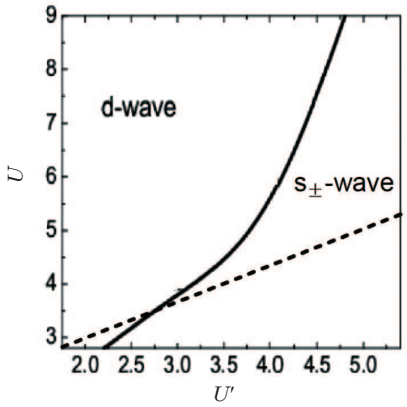


Fig. 14. The U–U' phase diagram of the s-wave and d-wave superconducting states for $J = J' = 1.0$. The dashed line is the boundary separating the regions of $U > U'$ and $U' < U$. Usually, the region $U > U'$ is physically realized.

The physical reason for the pairing symmetry realized here is the same as that for the $d_{x^2-y^2}$-wave pairing in the two-dimensional Hubbard model on the square lattice applied to high-T_c cuprates, as discussed in Subsection 3.2. Namely, for a repulsive pairing symmetry, the superconducting gap will satisfy the condition $\Delta(\boldsymbol{k})\Delta(\boldsymbol{k}+\boldsymbol{Q}) < 0$ to obtain the largest eigenvalue λ of the Eliashberg equation. Since the inter-band spin fluctuation has peaks around $(\pm\pi, 0)$ and $(0, \pm\pi)$, which are the nesting wave vectors connecting the hole and the electron Fermi pockets, the gap will have an opposite sign between these two Fermi pockets. This condition in fact leads to two candidates of the pairing symmetry. One is the $s_{\pm}$-wave shown in Figs. 12(c) and 12(d). The other is the d_{xy}-wave shown in Figs. 13(c) and 13(d). In the two cases, the electron and hole Fermi pockets connected by $(\pi, 0)$ have the opposite sign in the pairing gap. But, the gap function of each Fermi pocket has the same sign in the former case, while the sign changes in the latter case. When there is only the $(\pi, 0)$ spin fluctuation, the $s_{\pm}$-wave state would be energetically favored as it opens a full gap around the Fermi pockets. However, the additional $(0.5\pi, 0.5\pi)$ spin fluctuation emerges for a larger U. Therefore an additional condition $\Delta(\boldsymbol{k})\Delta(\boldsymbol{k}+\boldsymbol{q}_s) < 0$ with $\boldsymbol{q}_s = (0.5\pi, 0.5\pi)$ is also required, and it leads the gap function to change its sign within each Fermi pocket and thus induces a nodal d_{xy}-wave state.

Thus, a connection between the peak structure of the spin response and the pairing symmetry is established. The neutron scattering experiments carried out later on show that there is only one kind of spin fluctuation with a peak at $(\pi, 0)$ in most FeSCs,[55] therefore our theoretical results suggest that the $s_{\pm}$-wave is realized in these materials.

4.1.2. FLEX calculations based on the three-orbital model

As discussed in Section 2, it has been argued that at least a three-orbital model is needed to account for the main characters in the energy band. To test the stability of the results obtained using the two-band model, we have studied the spin fluctuations and superconducting pairing in the three-orbital model[28] as described in Subsection 2.2.

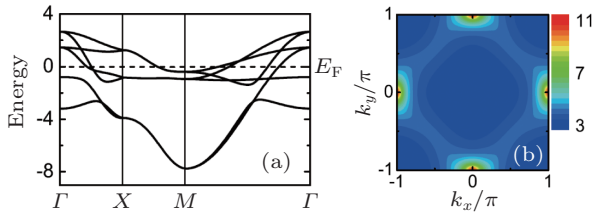


Fig. 15. (a) The energy band structure in the folded BZ in the three-orbital (d_{xz}, d_{yz}, d_{xy}) model. (b) The spin susceptibilities calculated with the FLEX approximation for $U = 3.0$ and $J = 0.2U$ at $T = 0.02$.[28]

The energy band and the static spin susceptibility with parameters $t_1 = 0.7$, $t_2 = -1.0$, $t_3 = -0.8$, $t_4 = -0.6$, $t_5 = -0.3$, $t_6 = 0.2$, $t_7 = 0.35$, $t_8 = 0$, $\Delta_{xy} = 0$, and $\mu = 1.15$ are shown in Fig. 15. Similar to that obtained in the two-band model, the spin susceptibility shows four peaks around points $(\pm\pi, 0)$ and $(0, \pm\pi)$, which arise from the nesting between the hole and the electron pockets. With this kind of spin fluctuations, we find that the eigenvalue λ of the Eliashberg equation (Eq. (31)) has the maximum value in the spin-singlet pairing channel. The obtained gap functions of the hole and the electron bands for 10% electron doping and 20% hole doping are shown in Fig. 16. It can be seen that the gap exhibits the $s_{\pm}$-wave character, which is nodeless around all the Fermi pockets and changes sign between the hole and the electron Fermi pockets. It is also noted that the pairing symmetry is similar for both the electron doped and the hole doped systems. Thus, the spin fluctuation and the superconducting pairing symmetry calculated with the FLEX approximation in the three-orbital

model show qualitatively the same results with those in the two-orbital model.[53]

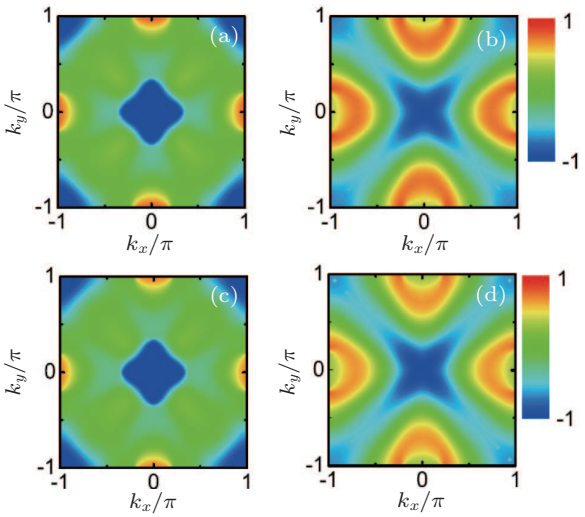


Fig. 16. Pairing gap functions in the one-Fe/cell BZ for $U = 3.0$ and $J = 0.2U$ at $T = 0.02$ for 10% electron doping and 20% hole doping: (a) $\Delta_{\rm hh}$ for electron doping, (b) $\Delta_{\rm ee}$ for electron doping, (c) $\Delta_{\rm hh}$ for hole doping, (d) $\Delta_{\rm ee}$ for hole doping.[28]

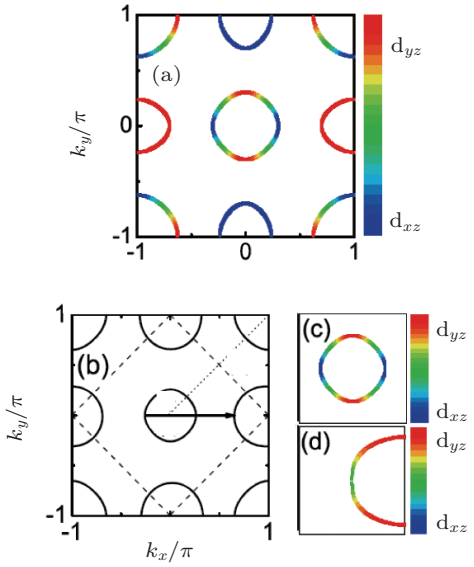


Fig. 17. (a) The weights of the d_{xz} and d_{yz} orbital contributions to the FS for the two-orbital model, which are shown by different colors. (b) The FS of the three-orbital model in the unfolded BZ. (c) and (d) Replot of the hole and electron Fermi pockets shown in panel (b), and different colors represent the weights of different orbitals.

The main difference between the two-orbital model and the three-orbital model exhibits in the orbital contributions to the corresponding FS. As shown in Fig. 17, in the two-orbital model,[25] the electron Fermi pocket near the $(\pi,0)$ point is composed of one orbital d_{yz} and the hole Fermi pocket around the $(0,0)$ point is the mix of both the d_{yz} and the d_{xz} orbitals. Because that portion of the hole Fermi pocket connected by the nesting wavevector $(\pi,0)$ is basically of the d_{xz} orbital character (see Fig. 17), the inter-band spin fluctuation coming from this nesting is in fact the inter-orbital particle–hole scattering between the d_{xz} and the d_{yz} orbitals. In the three-orbital model, the orbital composition of the hole Fermi pocket is the same as that in the two-orbital model, and the only difference is that the electron Fermi pocket now is a mix of the d_{yz} and the d_{xy} orbitals. Thus, the inter-band spin fluctuation with the wavevector $(\pi,0)$ involves both the inter-orbital scattering between the d_{xz} and the d_{yz} orbitals, and that between the d_{xz} and the d_{xy} orbitals. Though there is this difference, the inter-band spin fluctuation is sensitive to the nesting property of the FS, which is qualitatively the same in the two cases, so they result in the similar properties of the spin fluctuation. On the other hand, the $s_{\pm}$-wave pairing is mediated by the inter-band spin fluctuation and is resulted from the condition $\Delta(\boldsymbol{k})\Delta(\boldsymbol{k}+\boldsymbol{Q}) < 0$. Therefore, the similar spin fluctuations with the same wavevector $\boldsymbol{Q}$ will give the same pairing symmetry. In fact, this argument is also applied to the analysis for the more complicated five-orbital model discussed in the following.

4.1.3. Results of RPA and FRG based on the five-orbital models

Weak-coupling random phase approximation approaches to the pairing symmetry of iron-based superconductors have also predicted the $s_{\pm}$ paring symmetry based on the five-orbital models.[56,57] Graser *et al.* have performed a comprehensive study of the magnetic properties, pairing interactions, and pairing instabilities within a five-orbital tight-binding RPA model.[57] Figure 18 illustrates their results on the spin and charge susceptibilities for the undoped and 0.125 electron-doped compounds with $U = 1.65$. It is shown that the charge susceptibility is more than one order of magnitude smaller than the spin susceptibility, and has no pronounced structures in the momentum space (Fig. 18(d)). However, the spin susceptibility shows a strong momentum dependence. In the undoped compound, the main peak in the spin susceptibility is at wave vector $\boldsymbol{Q} = (\pi,0)$ with a secondary broad feature around (π,π) (Fig. 18(b)). With the electron doping, the peak at $\boldsymbol{Q} = (\pi,0)$ shifts a little bit to an incommensurate wave vector $\boldsymbol{Q}^* = (\pi,0.16\pi)$ (Fig. 18(c)). This shift can be attributed to an imperfect nesting of the hole- and electron-FS sheets due to the opposite growthes of the electron and hole sheets with doping, as shown in Fig. 18(a).

They also constructed the pairing vertices from the generalized RPA susceptibilities, and calculated the pairing eigenvalues for the dopings corresponding to undoped and electron-doped materials for a variety of interaction parameters. The results showed that the pairing interaction arises mainly from the exchange of spin fluctuations. They found that there are two leading pairing channels depending on the Coulomb interaction U, the extended s-wave symmetry and the $d_{x^2-y^2}$-wave symmetry, as shown in Fig. 19. The extended s-wave

state here is characterized by a) a sign change on the electron Fermi pockets with nodal points and b) a change of average sign on the electron pockets relative to that on the hole pockets (Fig. 19(b)). In particular, they showed that, within the parameter space explored, the anisotropic sign-changing s-wave state and the $d_{x^2-y^2}$ state are nearly degenerate due to the near nesting of the Fermi surface pockets (ee also Fig. 19(a)).

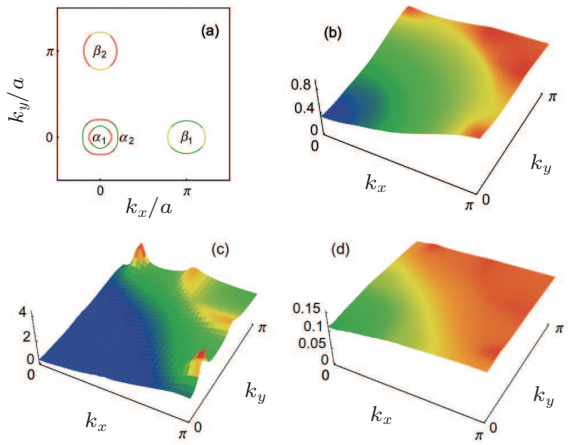


Fig. 18. (a) FS sheets of the five-orbital model for the undoped compound. (b) The bare spin susceptibility $\chi^s(\boldsymbol{k})$ calculated for the undoped five-orbital model. (c) The spin susceptibility for the 0.125 electron-doped compound. (d) The charge susceptibility for the 0.125 electron-doped compound.[57]

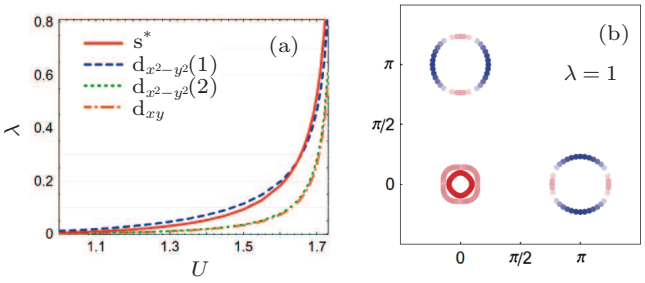


Fig. 19. (a) The eigenvalues and eigenfunctions for the electron-doped compound with $U = U'$ and $J = J' = 0$. (b) Color-coded plot of the extended $s_\pm$ wave.[57]

Wang *et al.*[58] have studied the pairing problem using a similar five-orbital effective energy band based on the functional renormalization group (FRG) approach. For both the electron and hole doped cases, they found that the leading pairing channel has an s-wave symmetry. In contrast, non-s-wave symmetries such as d-wave or triplet pairing are not favored (see Fig. 20). Thus, they predicted that the $s_\pm$ wave is the pairing symmetry of iron-based superconductors, which is consistent with the results of the FLEX calculations discussed above. With their interaction parameters, they found that there are no gap nodes on the whole FS, but there is a significant variation in the magnitude of the gap. By monitoring the growth of the renormalized vertex function, they found that the pairing instability is driven by the inter-band spin fluctuations.

It should be emphasized that the theories discussed above are all based on the itinerant-electron models, which are assumed based on the observation of the metallic behaviors of the parent compounds. There are also some theories based on the localized-spin models, such as the t–J_1–J_2 models,[59–61] which can be viewed as the strong coupling limit of the itinerant-electron models. In fact, the studies based on the localized-electron models also find that the most favorable superconducting pairing state is of the $s_\pm$-wave symmetry. In addition, at the self-consistent mean-field level, the magnetism in the FeAs stoichiometric compound and the interplay between magnetism and superconductivity upon doping have been investigated by self-consistently solving the Bogoliubov–de Gennes equations based on the two-orbital model with the inclusion of the on-site Coulomb interactions.[62] In the undoped system, it is shown that the collinear AFM spin-density-wave state is realized, namely, the local spin moments M_i antiferromagnetically aline along the x direction but ferromagnetically aline along the y direction in the real space. After the Fourier transformation of M_i, one gets an SDW order with wavevector $\boldsymbol{Q} = (\pi, 0)$, which is consistent with the experimental results in the undoped systems.[12] With doping, it is shown that the superconducting order parameter with $s_\pm = \Delta_0 \cos(k_x)\cos(k_y)$ symmetry is the most favorable pairing in both the electron- and hole-doped cases.[62] These results support the suggestion of the magnetic origin of the superconductivity in FeSCs.

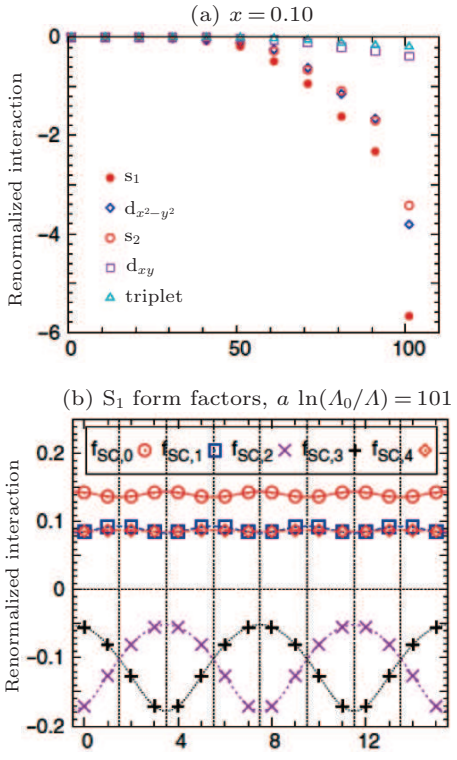


Fig. 20. Illustration of the FRG results for the 10% electron doping. (a) Evolution of the scattering amplitude in the top four attractive Cooper channels. (b) The gap function associated with the most attractive pairing channel. Here subscripts 0–4 label five Fermi surfaces.[58]

4.1.4. Experiment to probe the sign change of the gap function: spin resonance in neutron scattering

Though the superconducting gaps measured in experiments may vary among some different families of FeSCs and the experimental results obtained using different techniques may vary between a nodeless gap and a node gap, most experimental measurements have suggested that the $s_{\pm}$ superconducting gap is the most possible candidate in most of the families having both the electron and hole Fermi pockets. The $s_{\pm}$ superconducting gap has two features: (I) a nodeless gap on each of the electron and hole Fermi pockets and (II) opposite signs of the gaps between the electron and hole Fermi pockets. The detection of the magnitude of the energy gap has been carried out by angle-resolved photoelectron spectroscopy (ARPES) measurements,[63–67] in which the nodeless and nearly isotropic superconducting gaps on both the electron and hole Fermi pockets have been observed. This gives the first direct evidence of the possible $s_{\pm}$ pairing symmetry, for example in 122 system.[63] However, the ARPES measurements can not identify the sign of the superconducting gap. Up to now, the typical probe of the sign change of the gap function comes from the inelastic neutron scattering (INS) measurements, with which a so-called spin resonance has been identified in the superonducting state. This spin resonance is related to the property of spin fluctuations and is considered to be phase sensitive to the gap function, so we will give a brief discussion on it.

The spin resonance was in fact first found in high-T_c cuprates by INS experiments,[68,69] in which a resonance peak at the AFM wavevector $\boldsymbol{Q} = (\pi, \pi)$ appeared in the frequency dependence of the imaginary part of the spin susceptibility. Theoretically, the origin of the spin resonance is ascribed to a collective spin excitation mode in the weak coupling scheme,[70–74] which emerges at the pole of the RPA renormalized spin susceptibility, i.e., $1 + V_{\boldsymbol{Q}} \mathrm{Re}\chi_0(\boldsymbol{Q}, \omega) = 0$ and negligibly small $\mathrm{Im}\,\chi_0(\boldsymbol{Q}, \omega)$, with χ_0 the bare spin susceptibility and $V_{\boldsymbol{Q}}$ the interaction vertex. That the spin resonance appears only in the superconducting state has important implication for the properties of the superconducting gap. At low temperatures, the creation of Bogoliubov quasiparticle pairs gives the main contributions to χ_0, and the coherence factor for this process is

$$1 - \frac{\varepsilon(\boldsymbol{k})\varepsilon(\boldsymbol{k}+\boldsymbol{Q}) + \Delta(\boldsymbol{k})\Delta(\boldsymbol{k}+\boldsymbol{Q})}{E(\boldsymbol{k})E(\boldsymbol{k}+\boldsymbol{Q})} \approx 1 - \frac{\Delta(\boldsymbol{k})\Delta(\boldsymbol{k}+\boldsymbol{Q})}{|\Delta(\boldsymbol{k})||\Delta(\boldsymbol{k}+\boldsymbol{Q})|}, \tag{36}$$

where $\varepsilon(\boldsymbol{k})$ is the single-particle energy measured from the Fermi level, which is approximated to be zero because the quasiparticle pairs occur near the Fermi surface, and $E(\boldsymbol{k}) = \sqrt{\varepsilon^2(\boldsymbol{k}) + \Delta^2(\boldsymbol{k})}$. This suggests that the necessary condition for the appearance of the spin resonance is $\Delta(\boldsymbol{k})\Delta(\boldsymbol{k}+\boldsymbol{Q}) < 0$, so that the coherence factor is appreciable. In high-T_c cuprates, the superconducting gap has the $d_{x^2-y^2}$-wave symmetry, as shown in Fig. 9. The gap function connected by $\boldsymbol{Q} = (\pi, \pi)$ changes sign, so the coherence factor is approximately 1, thus this necessary condition is satisfied.

For the multi-orbital model, such as that for iron-based superconductors, the spin susceptibility within RPA has a matrix form.[75–77] Therefore, the pole condition is determined by $\det|\boldsymbol{I} - \hat{\boldsymbol{V}}\hat{\chi}_0(\boldsymbol{q}, \omega)|$, in which both the intra-band and the inter-band spin excitations are included in $\hat{\chi}_0$. The inter-band spin fluctuations have a strong peak around $(\pi, 0)$, which makes a main contribution and leads to an enhancement of $\hat{\chi}_0(\boldsymbol{Q}_s, \omega)$ with $\boldsymbol{Q}_s = (\pi, 0)$. For the $s_{\pm}$-wave gap which is mediated by the inter-band spin fluctuations, the condition $\Delta(k)\Delta(\boldsymbol{k} + \boldsymbol{Q}_s) < 0$ is satisfied, so the spin resonance is expected. Of course, the fulfillment of the resonance condition depends still on the details of the nesting property between the electron and hole Fermi pockets and the interaction vertex. The numerical calculations have shown that the well-defined spin resonance occurs only for the $s_{\pm}$-wave pairing, and is absence for d-wave pairings.[75–77]

Figure 21 is an example of INS results for $Ba_{0.6}K_{0.4}Fe_2As_2$ with $T_c = 38$ K.[78] A spin resonance peak in the superconducting state can be identified at $\boldsymbol{Q} = 1.15$ Å^{-1} corresponding to momentum $(\pi, 0)$, which is the right $\boldsymbol{Q}_s$ discussed above. Thus, it provides an evidence of the sign change in the gaps between the electron and hole Fermi pockets. Together with the ARPES results, the observation of the spin resonance peak in neutron scattering experiments gives a phase-sensitive evidence for the $s_{\pm}$-wave gap. Up to now, in many FeSCs,[79–82] the neutron resonance peak has been observed in the superconducting state. In addition, we note that the quasiparticle interference measurements,[83] in which the appearance of the interference peak also depends on the sign change of the gaps between different parts of FS,[84] also suggest an $s_{\pm}$ superconducting gap.

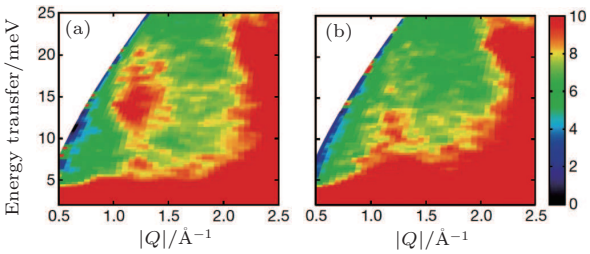


Fig. 21. Inelastic neutron scattering result of $Ba_{0.6}K_{0.4}Fe_2As_2$ measured at (a) 7 K and (b) 50 K, temperatures below and above T_c, respectively. The increase of scattering centered at energy 14 meV and momentum 1.15 Å^{-1} at 7 K compared to 50 K is ascribed to a spin resonance mode associated with the superconductivity that develops below $T_c = 38$ K.[78]

4.2. Systems with only electron pockets

A new family of iron-based superconductors, $A_xFe_{2-y}Se_2$ (A = K, Rb, Cs) discovered in 2010 with T_c higher than 30 K, has attracted much attention recently,[85–88] since there is only electron-like FS and no hole-like FS.[89–91]

The absence of the hole pockets formally violates the nesting condition between the hole and electron pockets, so the inter-band $(\pi,0)$ spin fluctuation and consequently the $s_\pm$ pairing symmetry are not expected. In this case, the five-orbital tight-binding model obtained by fitting to the LDA calculation[92] (see Fig. 22(a)) will give two sets of nesting wavevectors (π,π) and $(\pi,0.6\pi)$ (see Fig. 22(b)). According to the idea of the spin-fluctuation mediated superconductivity as described above, a $d_{x^2-y^2}$-wave pairing gap is naturally realized because the electron Fermi pockets connected by (π,π) and $(\pi,0.6\pi)$ should change sign (see Figs. 22(b) and 22(c)). Indeed, the weak-coupling calculations, including the FRG,[92] RPA,[93] and our FLEX approximation,[94] all suggest a dominant $d_{x^2-y^2}$-wave gap.

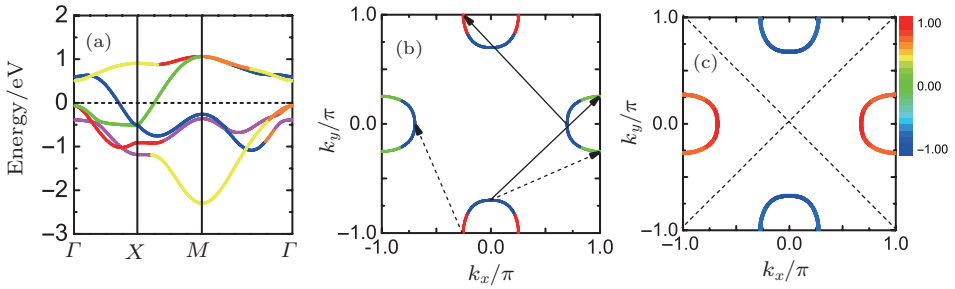


Fig. 22. (a) The energy band structure of the five-orbital model and (b) the FS in the unfolded BZ for 0.3 electron doping, the colors indicate the majority orbital characters (red: d_{xz}, green: d_{yz}, blue: d_{xy}, yellow: $d_{x^2-y^2}$, pink: d_{z^2}, orange: d_{xz} and d_{yz} with the same weight).[94] The solid lines with an arrow in panel (b) indicate the weak nesting vectors (π,π) and $(-\pi,\pi)$, and the dashed lines with an arrow indicate the weak nesting vectors $(\pi,0.6\pi)$ and $(-0.6\pi,\pi)$. (c) The most favorable $d_{x^2-y^2}$-wave gap as replot from Fig. 25(b), where the dotted lines denote the gap nodes.

Experimentally, the ARPES measurements have reported a nodeless superconducting gap on the large electron Fermi pockets around the $(\pi,0)$ point in these materials.[89–91] On the other hand, the nuclear magnetic resonance (NMR) experiments suggested an s_{+-}-wave pairing symmetry,[95,96] which is consistent with the isotropic gaps reported by ARPES. And, similar conclusions of the nodeless superconducting gap have been obtained from the muon spin spectroscopy experiment[97] and the specific heat measurement.[98] Because of the pocket structure of the electron FS and the absence of the FS around the $(0,0)$ point, the $d_{x^2-y^2}$-wave gap, which has nodes along the diagonal directions, does not show nodes on the FS, as shown in Fig. 22(c). So, the above experiments do not rule out the $d_{x^2-y^2}$-wave gap. The decisive experiment which rules out the $d_{x^2-y^2}$-wave symmetry is further ARPES measurements on the gap magnitude of the small electron Fermi pocket around the $(0,0)$ point, which still show an isotropic superconducting gap.[99,100] Therefore, the usual weak-coupling theory based on the itinerant spin fluctuation fails to account for the experimental measurements on the superconducting gap.

On the other hand, though the INS measurements reported a spin resonance in the superconducting state at $\boldsymbol{Q} \approx (\pi,\pi/2)$,[101–103] which is close to $(\pi,0.6\pi)$ and is consistent with the theoretical prediction of the spin resonance with the d-wave pairing symmetry,[93] another strong spin excitation near $(\pi,0)$ was also observed recently in the superconducting state.[103] Because of the absence of the hole Fermi pockets, this $(\pi,0)$ spin fluctuation is hard to understand based on the nesting between the electron and hole Fermi pockets. While the FLEX calculation based on the itinerant picture, which includes the on-site Coulomb interactions, has shown a broad peak around (π,π) in the spin susceptibility, as shown in Fig. 23, which is not observed in INS experiments.

In view of these deficiencies, we have studied the spin fluctuations and paring symmetry in $A_xFe_{2-y}Se_2$ with the FLEX approximation by including the next-nearest-neighbor (NNN) antiferromagnetic coupling J_2 which is a magnetic interaction from the localized model, together with the on-site Coulomb interaction which describes the itinerant nature of electrons.[94]

Figure 23 presents the evolution of spin fluctuations with the NNN antiferromagnetic coupling J_2. For $J_2 = 0$, as discussed above, a broad peak around (π,π) appears, together with four satellite peaks at $(\pi,\pm0.6\pi)$ and $(\pm0.6\pi,\pi)$ which arise from the FS nestings as illustrated in Fig. 22(b). When the J_2 term is turned on, the broad peak around (π,π) decreases rapidly, and the four satellite peaks are enhanced and move towards $(0,\pm\pi)$ and $(\pm\pi,0)$, as shown in Figs. 23(b)–23(d). As J_2 favors the diagonal antiferomagnetic order in the square lattice of Fe, it competes with the spin fluctuations coming from the nesting of FS. Thus, an enough large J_2 can

suppress the spin fluctuations from the nesting effect of FS and produce new characteristics in the spin fluctuations. An important point here is that we do not need a large J_2 (comparing to the band width 4 eV) to change the pattern of spin fluctuations. We find that when $J_2 > 0.04$ eV, the peak at (π,π) is completely suppressed. And the $(\pi,0)$ spin excitations observed in $Rb_{0.82}Fe_{1.68}Se_2$[103] also emerge for $J_2 > 0.04$ eV. In addition, for 0.03 eV $< J_2 <$ 0.05 eV, the peaks around $(\pm\pi,\pm 0.6\pi)$ and $(\pm 0.6\pi,\pm\pi)$ move to about $(\pm\pi,\pm 0.5\pi)$ and $(\pm 0.5\pi,\pm\pi)$, respectively. Therefore, the combined effect of the itinerant spin fluctuations and the localized moment gives rise to the spin excitations, which is consistent with the neutron scattering experiments.[101,103]

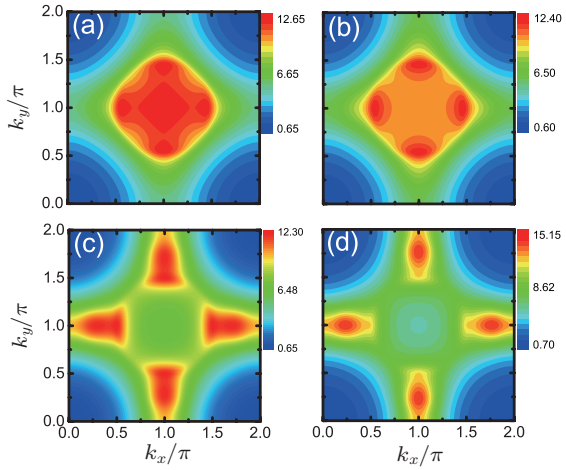


Fig. 23. Physical spin susceptibilities for different NNN antiferromagnetic coupling J_2: (a) $J_2 = 0$, (b) $J_2 = 0.01$ eV, (c) $J_2 = 0.04$ eV, (d) $J_2 = 0.05$ eV.[94]

The paring functions corresponding to the two leading eigenvalues have the extended s-wave and d-wave symmetries. In Fig. 24, we show these eigenvalues as a function of J_2 for 0.3 electron doping corresponding to $K_{0.6}Fe_2Se_2$. It is shown that the s-wave pairing state is dominant over the d-wave state when $J_2 > 0.045$ eV. This value of J_2 is comparable to the experimental value obtained from the INS measurement.[104] The gap functions on FS for the extended s-wave and d-wave symmetries corresponding to two representative values of J_2 are shown in Fig. 25. The extended s-wave gap shows no node on the Fermi surface. Moreover, after the Fourier transformation of this gap function into real space, we find that it can be fit well into the form $\Delta(\boldsymbol{k}) = \cos(k_x)\cos(k_y)$,[94] which is the $s_\pm$ pairing symmetry in iron arsenide, though now it has no hole Fermi pocket. This kind of $s_\pm$ pairing symmetry also has no node around the small momentum around $(0,0)$, so it is consistent with the ARPES experiments. We note that the same conclusion of the pairing symmetry in this system has also been obtained based on an effective Hamiltonian approach[105] and a functional renomalization group study.[106]

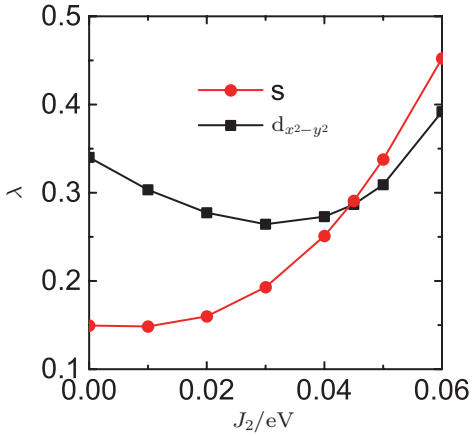


Fig. 24. The J_2 dependence of eigenvalues for the s-wave and d-wave solutions of the Eliashberg equation with $U = 1.2$ eV, $V = 0.35$ eV, $J_H = 0.2$ eV, and $T = 0.008$ eV.[94]

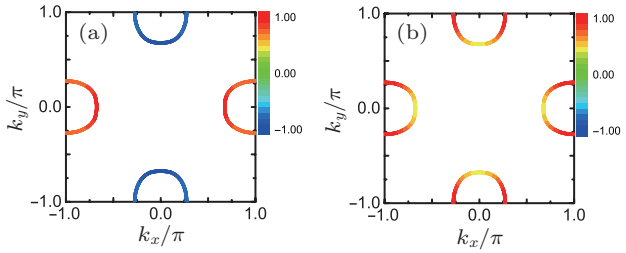


Fig. 25. The most favorable pairing functions on FS for (a) $J_2 = 0$ and (b) $J_2 = 0.05$.[94]

From Fig. 24, we also note that the d-wave and s-wave states are nearly degenerate around $J_2 = 0.045$ eV, thus the possible s + id pairing state may emerge. Although the pure s-wave pairing state does not give a spin resonance, the mixed s + id pairing state does give a spin resonance as observed in the INS experiments.[107]

5. Summary

We have tried to summarize the results on the spin fluctuation and superconducting pairing symmetry in iron-based superconductors based on the weak-coupling scenario. It is shown that an $s_\pm$-wave state mediated by spin fluctuations is the favorable superconducting pairing state, which shares the same underlying physics as the spin-fluctuation-mediated $d_{x^2-y^2}$ superconducting pairing in high-T_c cuprates. Though it is consistent with most available experiments, there are also some experimental results which are not consistent with the nodeless $s_\pm$-wave gap. In fact, the iron-based superconductors are complicated because of the multi-orbital nature of the energy band and the sensitivity of some physical properties to the compositions of materials. Therefore, further extensive studies are needed.

References

[1] Kamihara Y, Hiramatsu H, Hirano M, Kawamura R, Yanagi H, Kamiya T and Hosono H 2006 *J. Am. Chem. Soc.* **128** 10012

[2] Kamihara Y, Watanabe T, Hirano M and Hosono H 2008 *J. Am. Chem. Soc.* **130** 3296
[3] Chen X H, Wu T, Wu G, Liu R H, Chen H and Fang D F 2008 *Nature* **453** 761
[4] Chen G F, Li Z, Wu D, Li G, Hu W Z, Dong J, Zheng P, Luo J L and Wang N L 2008 *Phys. Rev. Lett.* **100** 247002
[5] Wen H H, Mu G, Fang L, Yang H and Zhu X Y 2008 *Europhys. Lett.* **82** 17009
[6] Ren Z A, Lu W, Yang J, Yi W, Shen X L, Zheng C, Che G C, Dong X L, Sun L L, Zhou F and Zhao Z X 2008 *Chin. Phys. Lett.* **25** 2215
[7] Rotter M, Tegel M and Johrendt D 2008 *Phys. Rev. Lett.* **101** 107006
[8] Wang X C, Liu Q Q, Lv Y X, Gao W B, Yang L X, Yu R C, Li F Y and Jin C Q 2008 *Solid State Commun.* **148** 538
[9] Hsu F C, Luo J Y, Yeh K W, Chen T K, Huang T W, Wu P M, Lee Y C, Huang Y L, Chu Y Y, Yan D C and Wu M K 2008 *Proc. Natl. Acad. Sci. USA* **105** 14262
[10] Wang C, Li L, Chi S, Zhu Z, Ren Z, Li Y, Wang Y, Lin X, Luo Y, Jiang S, Xu X, Cao G and Xu Z A 2008 *Europhys. Lett.* **83** 67006
[11] Cheng P, Shen B, Mu G, Zhu X, Han F, Zeng B and Wen H H 2009 *Europhys. Lett.* **85** 67003
[12] de la Cruz C, Huang Q, Lynn J W, Li J, Ratcliff II W, Zarestky J L, Mook H A, Chen G F, Luo J L, Wang N L and Dai P C 2008 *Nature* **453** 899
[13] Rotter M, Tegel M and Johrendt D 2008 *Phys. Rev. B* **78** 020503
[14] Huang Q, Qiu Y, Bao W, Green M A, Lynn J W, Gasparovic Y C, Wu T, Wu G and Chen X H 2008 *Phys. Rev. Lett.* **101** 257003
[15] Li S L, de la Cruz C, Huang Q, Chen G F, Xia T L, Luo J L, Wang N L and Dai P C 2009 *Phys. Rev. B* **80** 020504
[16] Bao W, Qiu Y, Huang Q, Green M A, Zajdel P, Fitzsimmons M R, Zhernenkov M, Chang S, Fang M H, Qian B, Vehstedt E K, Yang J H, Pham H M, Spinu L and Mao Z Q 2009 *Phys. Rev. Lett.* **102** 247001
[17] Li S L, de la Cruz C, Huang Q, Chen Y, Lynn J W, Hu J P, Huang Y L, Hsu F C, Yeh K W, Wu M K and Dai P C 2009 *Phys. Rev. B* **79** 054503
[18] Bao W, Huang Q Z, Chen G, Green M, Wang D M, He J B and Qiu Y M 2011 *Chin. Phys. Lett.* **28** 086104
[19] Ye F, Chi S, Bao W, Wang X F, Ying J J, Chen X H, Wang H D, Dong C H and Fang M H 2011 *Phys. Rev. Lett.* **107** 137003
[20] Lu X, Gretarsson H, Zhang R, Liu X, Luo H, Tian W, Laver M, Yamani Z, Kim Y J, Nevidomskyy A H, Shi Q and Dai P C 2013 *Phys. Rev. Lett.* **110** 257001
[21] Chen H, Ren Y, Qiu Y, Bao W, Liu R H, Wu G, Wu T, Xie Y L, Wang X F, Huang Q and Chen X H 2009 *Europhys. Lett.* **85** 17006
[22] Damascelli A, Hussin Z and Shen Z X 2003 *Rev. Mod. Phys.* **75** 473
[23] Singh D J 2008 *Phys. Rev. B* **78** 094511
[24] Mazin I I, Singh D J, Johannes M D and Du M H 2008 *Phys. Rev. Lett.* **101** 057003
[25] Raghu S, Qi X L, Liu C X, Scalapino D J and Zhang S C 2008 *Phys. Rev. B* **77** 220503
[26] Lee P A and Wen X G 2008 *Phys. Rev. B* **78** 144517
[27] Daghofer M, Nicholson A, Moreo A and Dagotto E 2010 *Phys. Rev. B* **81** 014511
[28] Yu S L, Kang J and Li J X 2009 *Phys. Rev. B* **79** 064517
[29] Long M S, Hu L B and LiMing W 2010 *Eur. Phys. J. B* **75** 205
[30] Kanamori J 1963 *Prog. Theor. Phys.* **30** 275
[31] Castellani C, Natoli C R and Ranninger J 1978 *Phys. Rev. B* **18** 4945
[32] Tang H, Plihal M and Mills D L 1998 *J. Magn. Magn. Mater.* **187** 23
[33] Berk N F and Schrieffer J R 1966 *Phys. Rev. Lett.* **17** 433
[34] Brinkman W F, Serene J W and Anderson P W 1974 *Phys. Rev. A* **10** 2386
[35] Leggett A J 1975 *Rev. Mod. Phys.* **47** 331
[36] Stewart G R 1984 *Rev. Mod. Phys.* **56** 755
[37] Joynt R and Taillefer L 2002 *Rev. Mod. Phys.* **74** 235
[38] Powell B J and McKenzie R H 2011 *Rep. Prog. Phys.* **74** 056501
[39] Jérome D and Schulz H J 2002 *Adv. Phys.* **51** 293
[40] Lee P A, Nagaosa N and Wen X G 2006 *Rev. Mod. Phys.* **78** 17
[41] Armitage N P, Fournier P and Greene R L 2010 *Rev. Mod. Phys.* **82** 2421
[42] Paglione J and Greene R L 2010 *Nat. Phys.* **6** 645
[43] Johnston D C 2010 *Adv. Phys.* **59** 803
[44] Stewart G R 2011 *Rev. Mod. Phys.* **83** 1589
[45] Abrikosov A A, Gor'kov L P and Dzyaloshinskii L E 1975 *Methods of the Quantum Field Theory in Statistical Physics* (New York: Dover Publications)
[46] Scalapino D J, Loh E Jr and Hirsch J E 1986 *Phys. Rev. B* **34** 8190
[47] Bickers N E, Scalapino D J and White S R 1989 *Phys. Rev. Lett.* **62** 961
[48] Bickers N E and Scalapino D J 1989 *Ann. Phys.* **193** 206
[49] Baym G and Kadanoff L P 1961 *Phys. Rev.* **124** 287
[50] Baym G 1962 *Phys. Rev.* **127** 1391
[51] Takimoto T, Hotta T and Ueda K 2004 *Phys. Rev. B* **69** 104504
[52] Boeri L, Dolgov O V and Golubov A A 2008 *Phys. Rev. Lett.* **101** 026403
[53] Yao Z J, Li J X and Wang Z D 2009 *New J. Phys.* **11** 025009
[54] Vidberg H J and Serene J W 1977 *J. Low Temp. Phys.* **29** 179
[55] Dai P C, Hu J P and Dagotto E 2012 *Nat. Phys.* **8** 709
[56] Kuroki K, Onari S, Arita R, Usui H, Tanaka Y, Kontani H and Aoki H 2008 *Phys. Rev. Lett.* **101** 087004
[57] Graser S, Maier T A, Hirschfeld P J and Scalapino D J 2009 *New J. Phys.* **11** 025016
[58] Wang F, Zhai H, Ran Y, Vishwanath A and Lee D H 2009 *Phys. Rev. Lett.* **102** 047005
[59] Seo K, Bernevig B A and Hu J P 2008 *Phys. Rev. Lett.* **101** 206404
[60] Parish M M, Hu J P and Bernevig B A 2008 *Phys. Rev. B* **78** 144514
[61] Goswami P, Nikolic P and Si Q M 2010 *Europhys. Lett.* **91** 37006
[62] Jiang H M, Li J X and Wang Z D 2009 *Phys. Rev. B* **80** 134505
[63] Ding H, Richard P, Nakayama K, Sugawara K, Arakane T, Sekiba Y, Takayama A, Souma S, Sato T, Takahashi T, Wang Z, Dai X, Fang Z, Chen G F, Luo J L and Wang N L 2008 *Europhys. Lett.* **83** 47001
[64] Zhao L, Liu H Y, Zhang W T, Meng J Q, Jia X W, Liu G D, Dong X L, Chen G F, Luo J L, Wang N L, Lu W, Wang G L, Zhou Y, Zhu Y, Wang X Y, Xu Z Y, Chen C T and Zhou X J 2008 *Chin. Phys. Lett.* **25** 4402
[65] Terashima K, Sekiba Y, Bowen J H, Nakayama K, Kawahara T, Sato T, Richard P, Xu Y M, Li L J, Cao G H, Xu Z A, Ding H and Takahashi T 2009 *Proc. Natl. Acad. Sci. USA* **106** 7330
[66] Evtushinsky D V, Inosov D S, Zabolotnyy V B, Koitzsch A, Knupfer M, Büchner B, Viazovska M S, Sun G L, Hinkov V, Boris A V, Lin C T, Keimer B, Varykhalov A, Kordyuk A A and Borisenko S V 2009 *Phys. Rev. B* **79** 054517
[67] Kondo T, Santander-Syro A F, Copie O, Liu C, Tillman M E, Mun E D, Schmalian J, Bud'ko S L, Tanatar M A, Canfield P C and Kaminski A 2008 *Phys. Rev. Lett.* **101** 147003
[68] Rossat-Mignod J, Regnault L P, Vettier C, Bourges P, Burlet P, Bossy J, Henry J Y and Lapertot G 1991 *Physica C* **185** 86
[69] Fong H F, Keimer B, Anderson P W, Reznik D, Dogan F and Aksay I A 1995 *Phys. Rev. Lett.* **75** 316
[70] Bulut N and Scalapino D J 1996 *Phys. Rev. B* **53** 5149
[71] Li J X, Yin W G and Gong C D 1998 *Phys. Rev. B* **58** 2895
[72] Brinckmann J and Lee P A 1999 *Phys. Rev. Lett.* **82** 2915
[73] Li J X and Gong C D 2002 *Phys. Rev. B* **66** 014506
[74] Eschrig M 2006 *Adv. Phys.* **55** 47
[75] Korshunov M M and Eremin I 2008 *Phys. Rev. B* **78** 140509
[76] Maier T A and Scalapino D J 2008 *Phys. Rev. B* **78** 020514
[77] Maier T A, Graser S, Scalapino D J and Hirschfeld P 2009 *Phys. Rev. B* **79** 134520
[78] Christianson A D, Goremychkin E A, Osborn R, Rosenkranz S, LumsdenMD, Malliakas C D, Todorov I S, Claus H, Chung D Y, KanatzidisMG, Bewley R I and Guidi T 2008 *Nature* **456** 930
[79] Lumsden M D, Christianson A D, Parshall D, Stone M B, Nagler S E, MacDougall G J, Mook H A, Lokshin K, Egami T, Abernathy D L, Goremychkin E A, Osborn R, McGuire M A, Sefat A S, Jin R, Sales B C and Mandrus D 2009 *Phys. Rev. Lett.* **102** 107005
[80] Li S L, Chen Y, Chang S, Lynn J W, Li L, Luo Y, Cao G H, Xu Z A and Dai P C 2009 *Phys. Rev. B* **79** 174527
[81] Qiu Y, Bao W, Zhao Y, Broholm C, Stanev V, Tesanovic Z, Gasparovic Y C, Chang S, Hu J, Qian B, Fang M and Mao Z 2009 *Phys. Rev. Lett.* **103** 067008
[82] Shamoto S I, Ishikado M, Christianson A D, Lumsden M D, Wakimoto S, Kodama K, Iyo A and Arai M 2010 *Phys. Rev. B* **82** 172508
[83] Hanaguri T, Niitaka S, Kuroki K and Takagi H 2010 *Science* **328** 474
[84] Wang F, Zhai H and Lee D H 2009 *Europhys. Lett.* **85** 37005
[85] Guo J, Jin S, Wang G, Wang S, Zhu K, Zhou M H T and Chen X 2010 *Phys. Rev. B* **82** 180520
[86] Wang A F, Ying J J, Yan Y J, Liu R H, Luo X G, Li Z Y, Wang X F, Zhang M, Ye G J, Cheng P, Xiang Z J and Chen X H 2011 *Phys. Rev. B* **83** 060512

[87] Krzton-Maziopa A, Shermadini Z, Pomjakushina E, Pomjakushin V, Bendele M, Amato A, Khasanov R, Luetkens H and Conder K 2011 *J. Phys.: Condens. Matter* **23** 052203
[88] Fang M H, Wang H D, Dong C H, Li Z J, Feng C M, Chen J and Yuan H Q 2011 *Europhys. Lett.* **94** 27009
[89] Zhang Y, Yang L X, Xu M, Ye Z R, Chen F, He C, Xu H C, Jiang J, Xie B P, Ying J J, Wang X F, Chen X H, Hu J P, Matsunami M, Kimura S and Feng D L 2011 *Nat. Mater.* **10** 273
[90] Qian T, Wang X P, Jin W C, Zhang P, Richard P, Xu G, Dai X, Fang Z, Guo J G, Chen X L and Ding H 2011 *Phys. Rev. Lett.* **106** 187001
[91] Mou D, Liu S, Jia X, He J, Peng Y, Zhao L, Yu L, Liu G, He S, Dong X, Zhang J, Wang H, Dong C, Fang M, Wang X, Peng Q, Wang Z, Zhang S, Yang F, Xu Z, Chen C and Zhou X J 2011 *Phys. Rev. Lett.* **106** 107001
[92] Wang F, Yang F, Gao M, Lu Z Y, Xiang T and Lee D H 2011 *Europhys. Lett.* **93** 57003
[93] Maier T, Graser S, Hirschfeld P and Scalapino D J 2011 *Phys. Rev. B* **83** 100515
[94] Yu S L, Guo J and Li J X 2013 arXiv: 1305.1090 [cond-mat]
[95] Torchetti D A, Fu M, Christensen D C, Nelson K J, Imai T, Lei H C and Petrovic C 2011 *Phys. Rev. B* **83** 104508
[96] Kotegawa H, Hara Y, Nohara H, Tou H, Mizuguchi Y, Takeya H and Takano Y 2011 *J. Phys. Soc. Jpn.* **80** 043708
[97] Shermadini Z, Luetkens H, Khasanov R, Krzton-Maziopa A, Conder K, Pomjakushina E, Klauss H H and Amato A 2012 *Phys. Rev. B* **85** 100501
[98] Zeng B, Shen B, Chen G F, He J B, Wang D M, Li C H and Wen H H 2011 *Phys. Rev. B* **83** 144511
[99] Xu M, Ge Q Q, Peng R, Ye Z R, Jiang J, Chen F, Shen X P, Xie B P, Zhang Y, Wang A F, Wang X F, Chen X H and Feng D L 2012 *Phys. Rev. B* **85** 220504
[100] Wang X P, Richard P, Shi X, Roekeghem A, Huang Y B, Razzoli E, Qian T, Rienks E, Thirupathaiah S, Wang H D, Dong C H, Fang M H, Shi M and Ding H 2012 *Europhys. Lett.* **99** 67001
[101] Park J T, Friemel G, Li Y, Kim J H, Tsurkan V, Deisenhofer J, Krug von Nidda H A, Loidl A, Ivanov A, Keimer B and Inosov D S 2011 *Phys. Rev. Lett.* **107** 177005
[102] Friemel G, Park J T, Maier T A, Tsurkan V, Li Y, Deisenhofer J, Krug von Nidda H A, Loidl A, Ivanov A, Keimer B and Inosov D S 2012 *Phys. Rev. B* **85** 140511
[103] Wang M, Li C, Abernathy D L, Song Y, Carr S V, Lu X, Li S, Yamani Z, Hu J P, Xiang T and Dai P C 2012 *Phys. Rev. B* **86** 024502
[104] Wang M, Fang C, Yao D X, Tan G, Harriger LW, Song Y, Netherton T, Zhang C L, Wang M, Stone M B, TianW, Hu J P and Dai P C 2011 *Nat. Commun.* **2** 580
[105] Yang F, Wang F and Lee D H 2013 arXiv: 1305.0605 [cond-mat]
[106] Xiang Y Y, Yang Y, Wang W S, Li Z Z and Wang Q H 2013 arXiv: 1305.1806 [cond-mat]
[107] Maier T, Hirschfeld P and Scalapino D J 2012 arXiv: 1206.5235 [cond-mat]